Pure Appl. Geophys. 177 (2020), 3013–3037

https://doi.org/10.1007/s00024-019-02361-7

Pure and Applied Geophysics

Spatio-Seasonal Variations in Long-Term Trends of Offshore Wind Speeds Over the Black Sea; an Inter-Comparison of Two Reanalysis Data

Tunay Çarpar,[1] Berna Ayat,[2] and Burak Aydoğan[3]

Abstract—Spatio-seasonal variability of long-term trends in mean and 95th percentile wind speeds for the term between 1979 and 2016, over the Black Sea is presented. Our aim is to contribute the existing literature by presenting the inhomogeneous spatial distribution of the long-term trends in both moderate and severe wind speeds on a monthly basis. The analysis is conducted by using two different data; European Centre for Medium-Range Weather Forecasts-ERA-Interim and U.S. National Centers for Environmental Prediction-Climate Forecast System Reanalysis (CFSR) to perform a comparative analysis. The non-parametric Mann–Kendall and Sen's Slope methods are used to determine the trends and their significance over the Black Sea. CFSR winds presented higher interannual variability than the ERA-Interim. ERA-Interim indicates that annual mean and 95th percentile wind speeds have decreasing trends down to − 0.17%/year and − 0.20%/year in the Sea of Azov, while they have an increasing trend up to 0.35%/year and 0.38%/year in the eastern part, respectively. Results indicate that wind speeds are increasing over 28% ∼ 36% of the Black Sea surface area while the wind speeds are decreasing over 2% ∼ 4% of the surface area. Pacific North American Oscillation presented an influence almost all over the Black Sea with statistically significant correlation coefficients over 0.5. North Atlantic Oscillation dominates over the southwestern, western and northern Black Sea with inverse correlation coefficients over 0.6. ERA-Interim and CFSR data illustrated a similar distribution pattern over the Black Sea in means of the relation of variations in wind speeds to the teleconnection indices.

Keywords: Long-term trend, wind speed, Black Sea, teleconnection, spatiotemporal variability, monthly variability.

1. Introduction

Wind speed is the direct and indirect forcing for many natural processes such as storms (Zainescu et al. 2017), and coastal erosion (Healy 2018), ventilation of the water in the marine environment, coastal circulation (Shepherd et al. 2017), wind-wave generation (Rusu et al. 2014; Aydoğan and Ayat 2018), etc. Wind speed also affects marine activities such as seakeeping safety, stabilities of the offshore structures (Wang and Hwang 2001), marine transportation (Rusu et al. 2018), port operations (Athanasatos et al. 2014), tourism (Georgopoulou et al. 2018), fisheries (Masuda et al. 2014), renewable energy generation (Ganea et al. 2018; Aydoğan 2017), etc. Long-term changes in wind speed at coastal and offshore regions have great importance on the sustainability of natural processes and marine activities.

Long-term trends in 10 m-wind speeds (*U10*) have been studied at local (Li et al. 2011), regional (Troccoli et al. 2012; Jiang et al. 2010), and global scales (Young et al. 2011). For the evaluation of the *U10* variations at a local scale, local measurement data is sufficient (Tuller 2004). Regional and global scale evaluations require homogeneous time series that cover the study area with proper temporal and spatial details (Weisse and Gunther 2007). Zheng et al. (2016) presented spatial and seasonal variations of annual mean *U10* ($U10_m$) for the period between 1988 and 2011, focusing on a study area covering all of the global oceanic sea surfaces. The researchers reported that the $U10_m$ increased at a significant overall rate of 3.35 cm/s/year for the period 1988–2011 over the global oceanic sea-surface and the long-term trend values showed noticeable

[1] Istanbul Water and Sewerage Administration (ISKI), 34060 Eyüp/Istanbul, Turkey. E-mail: tcarpar@iski.gov.tr
[2] Department of Civil Engineering, Yildiz Technical University, 34220 Esenler/Istanbul, Turkey. E-mail: ayat@inm.yildiz.edu.tr
[3] Department of Civil Engineering, Gebze Technical University, 41400 Gebze/Kocaeli, Turkey. E-mail: baydogan@gtu.edu.tr

regional inhomogeneity. Sterl and Caires (2005) also studied spatiotemporal variations in *U10* over the global ocean and reported an increasing trend reaching up to the rate of 6 cm/s/year for $U10_m$ between 1971 and 2000 based on ERA40 reanalysis provided by European Center for Medium-Range Weather Forecasts (ECMWF). Authors found that 99th percentile *U10* increases at even a higher rate of 12 cm/s/year over some specific regions.

Long-term changes in *U10* over the Black Sea has also been studied intensively due to the need of both the sustainable marine activities in riparian countries and the preservation of its unique natural environment. Cakiroglu et al. (2017) analyzed measured wind data at seven coastal stations for the period between 1970 and 2010 and reported that the $U10_m$ changes at statistically significant rates of 2 cm/s/year and − 3 cm/s/year over the southwestern Black Sea and the southeastern Black Sea, respectively. Aydoğan (2017) presented the offshore wind power atlas of the Black Sea. The author used the ECMWF ERA-Interim reanalysis (ERA-I) to evaluate offshore wind energy potential within the basin for the 38 years between 1979 and 2016. The author compared the ERA-I data with the in situ measurements from two coastal station in the southwestern Black Sea and concluded that ERA-I data well matched with the observations. Comparison of U.S. National Centers for Environmental Prediction (NCEP) of National Oceanic and Atmospheric Administration (NOAA), Climate Forecast System Reanalysis (CFSR) reanalysis wind data with the in situ measurements at Gloria platform conducted by Rusu et al. (2018) reporting that the CFSR reanalysis data give slightly higher wind speeds than the measured ones at that location. Ganea et al. (2019) studied the temporal variations in *U10* at six nearshore locations along the Black Sea coastline based on ERA-I data for the term 1983–2017 in the frame of "Assessment of the Climate Change Effects on the Wave Conditions in the Black Sea (ACCWA)" project. Authors reported a statistically significant decreasing trend with a rate of 1 cm/s/decade in $U10_m$ for the northwestern Black Sea. Akpinar and Bingolbali (2016) analyzed the long-term variations of wind conditions in 33 coastal locations along the Black Sea coastline, excluding the offshore. Researchers used the CFSR wind fields for the term between 1979 and 2009. They reported that $U10_m$ have statistically significant increasing trends in the ranges of 0.398 cm/s/year—0.813 cm/s/year and 0.902 cm/s/year—1.337 cm/s/year, for the southeastern coasts of the Black Sea and around the Crimean Peninsula, respectively. Zainescu et al. (2017) studied storminess along the Danube Delta Coast since 1949 by analyzing wind data. Authors also revealed the relation of teleconnection patterns with the regional variability of sea storms and concluded that the North Atlantic Oscillation (*NAO*) has the highest correlation with the storminess of the Danube Delta Coast, however, for the last 10 years, the East Atlantic (*EA*) pattern and the East Atlantic/West Russia (*EA/WR*) pattern becomes more notable. Valchev et al. (2012) aimed to explore the trends for storminess in the western Black Sea for the years between 1948 and 2010. Authors conducted the temporal analysis of the variations of storminess and concluded that there is no statistically significant increasing or decreasing trend in the storminess over the western Black Sea.

Wind fields over the Black Sea basin are influenced by large scale atmospheric circulations controlled by the Siberian anticyclone, Mediterranean cyclonic activity, Azores anticyclone, and Island cyclone. Influence of the Siberian anticyclone manifests itself, especially in winter. In the eastern basin, dominated large scale atmospheric circulation is caused by the Azores anticyclone with an increasing impact during summer (Kubryakov et al. 2019). Another important cyclonic air flow is the Island cyclone which effects the wind climate in the Black Sea throughout the year (Efimov and Anisimov 2011; Rusu et al. 2014). Different height of mountainous ridges, North Anatolian Mountains along the southern coasts, the Caucasus Mountains along the eastern coasts, and the Crimean Mountains induce important impact on the windiness of the Black Sea since they interrupt the winds from the arc from south to east (Arkhipkin et al. 2014). Lowlands between the mountains and the narrow valleys cause high-velocity winds such as Novorossiyskaya Bora, occasionally (Rusu et al. 2014). Özsoy and Ünlüata (1997) reported two primary pathways for winter winds; one is moving northeastward direction over the Sea of Marmara originated from the Mediterranean Sea, and

the other one in eastward and southeastwards directions from the Romania. Detailed atmospheric setting of the Black Sea basin can be found in Özsoy and Ünlüata (1997), Surkova et al. (2013), Zecchetto and de Biasio (2007), and Kostianoy and Kosarev (2008).

Difficulties arise in the comparison and synthesis of the results due to the different data sources analyzed and different temporal coverages considered in the studies so far. Comparative studies for the long-term trends of wind speeds over the Black Sea becomes important in this regard. This kind of comparative analysis of wind speeds was conducted by Rusu et al. (2018) along the shipping routes in the Black Sea. Authors evaluated the wind conditions for the term between 1 January 1987 and 31 December 2009 based on the CFSR reanalysis data and the hindcast results provided by a Regional Climate Model (RCM) that were retrieved from European Domain-Coordinated Regional Climate Downscaling Experiment (EURO-CORDEX). Authors reported a good agreement between two data sources for the offshore sites and nearshore sites except for the southern part of the Black Sea. Rusu et al. (2018) evaluated the long-term trends in 95th percentile *U10* ($U10_{95}$) as well as the $U10_m$ and concluded that no statistically significant trend exists for both time series within the study period at the selected location (Gloria platform).

The variations of the wind speeds over the sea surfaces represent perceptible seasonal differences, which point out the necessity of seasonal analysis of wind speeds (Zheng et al. 2016). Seasonal variations of the wind speeds were also analyzed in recent studies (Rusu et al. 2018; Aydoğan 2017; Akpinar and Bingolbali 2016) indicating higher wind speeds during the winter months and lower wind activity during the summer months. Based on this finding, Velea et al. (2014) analyzed the frequency of extreme winds over the Black Sea surface by focusing on January for the period 2001–2009. The entire Black Sea basin was studied and western and northern areas found to have moderate and strong winds between 2001 and 2009.

Although the wind climate and the storminess in the Black Sea have been studied widely for different parts of the basin or some specific locations, the spatial variability of the long-term trends of wind speeds, their spatiotemporal variability in a monthly basis, correlations to the teleconnection indices have not been examined sufficiently.

In this study, we aimed to contribute the existing literature by conducting a spatiotemporal analysis of the long-term trends of *U10* over the whole Black Sea, both in terms of mean and severe states in a comparative manner by using two different widely used reanalysis data (ERA-I and CFSR) covering an extended time period of 38 years, from 01 January1979 to 31 December 2016. Spatio-seasonal variations of the long-term trends are studied on a monthly basis to enhance our understanding of the changes in windiness over the Black Sea. The relation of the temporal evolution of *U10* to climate indices are analyzed to have an insight into the causes of the characterized trends.

2. Data and Methodology

2.1. Study Area

The study area delimited by latitudes 40–48°N and longitudes 26–42°E, covers the Black Sea basin and the Sea of Azov as shown in Fig. 1. The Black Sea is surrounded by Ukraine from the north, Russia from the northeast, Georgia from the east, Turkey from the south, and Bulgaria and Romania from the west. Its surface area is 411,540 km^2 and its volume is 555,000 km^3 whereas the mean and maximum depths are 1315 m and 2258 m, respectively. The total length of the Black Sea coastline is $\sim$ 3400 km. The Black Sea is an enclosed basin connected to the Mediterranean through the Turkish Sea Strait System consisting of the Strait of Istanbul, the Sea of Marmara and the Dardanelles and the Sea of Azov via the Strait of Kerch. The Black Sea basin has intensive shipping activities between the important harbors of Europe, Asia, and Africa. The Black Sea is one of the most isolated divisions of the world ocean system and as a result of wind activity over the sea, heavy waves are observed (Onea and Rusu 2012). Black Sea basin is under the influence of air masses which come and pass over along various directions, because of its geographical location. As a consequence of its position, the Black Sea climate is

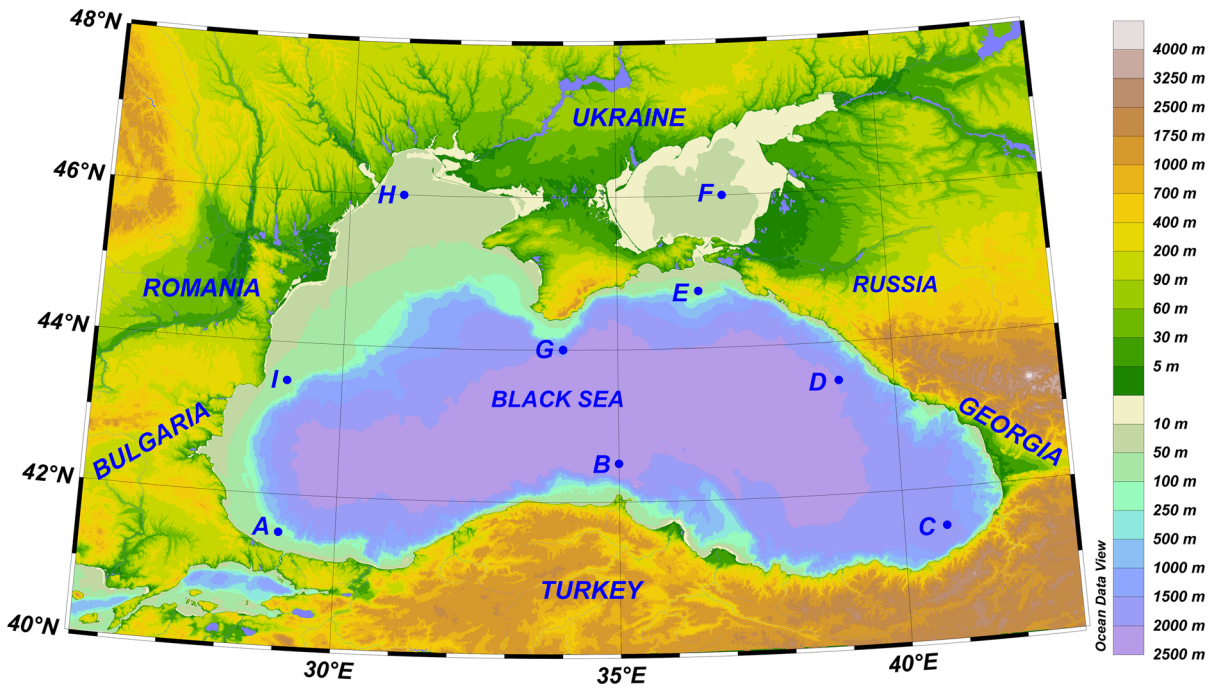

Figure 1
Study area: the Black Sea and the selected study sites

affected by continental, polar and marine tropical air fluxes from several directions. The marine tropical air mass flow results from southwest winds from the Mediterranean basin and in the winter, polar air masses coming from north and northeast lead to low temperatures and frequent storms over the Black Sea (Valchev et al. 2010).

Nine study sites are selected to study interannual variability of the moderate and severe wind conditions since this data cannot be presented spatially. These nearshore locations are chosen so that they distributed almost uniformly along the Black Sea coastline to cover most of the interannual variability patterns in the basin. These representative study sites are also chosen as major harbor locations where important marine activities are carrying out. Selected nearshore study sites and corresponding water depths are A (140 m), B (2100 m), C (1660 m), D (1910 m), E (71 m), F (12 m), G (1620 m), H (26 m), and I (84 m).

2.2. *Data*

In this study, two reanalysis data are used to explore the long-term trends in *U10* over the Black Sea consisting of ERA-I (Dee et al. 2011) and CFSR (Saha et al. 2010, 2014). Both reanalysis data over the Black Sea are processed for the same period of time between 01 January 1979 and 31 December 2016.

Both ERA-I and CFSR assimilates different data from various sources such as scatterometers, altimeters, satellite measurements, in situ meteorological observations, etc., with 12 h analysis periods. Historical information about the various climate parameters including wind velocities at different pressure levels, precipitation, evaporation, cloud cover, snowfall, temperature, spectral wave parameters, mean sea level, and many others can be obtained for global atmosphere, land and ocean.

ERA-I data is provided by the ECMWF for the period starting from 01 January 1979 to the present and the project will be terminated on 31 August 2019. ERA-I is generated by 4D variational assimilation of data from various sources. ERA-I uses the stability function of the bulk algorithm to compute air-sea fluxes given by Holtslag and de Bruin (1988) and Dyer (1974). The roughness length for momentum is computed from the coupled ocean wave model (Zhang et al. 2016). The near-surface u and

v components of wind velocity at 10 m height are obtained from ERA-I with a spatial resolution of 0.7° × 0.7° (∼ 80 km) from native T255 spectral grid and a temporal resolution of 6 h for this study.

CFSR reanalysis data covers the term from 01 January 1979 to the present. CFSR data is derived from 3D-Var assimilation of the various data based on a coupled atmosphere–ocean–land data assimilation system. The air-sea fluxes in the CFSR are derived from the model which uses the roughness lengths given by Zeng et al. (1998) for heat and moisture (Zhang et al. 2016). CFSR reanalysis data has a spatial resolution of 0.312°×0.312° (∼ 38 km) from native T382 spectral grid and near-surface u and v wind velocity components are obtained with a temporal resolution of 6 h for this study.

U10 data is constructed by using the wind velocity components from reanalysis data. Temporal and spatial resolutions and temporal coverages of the reanalysis data used in this study are presented in Table 1.

To have a comparable homogeneous spatial analysis of long-term changes in the *U10* data, both reanalysis data are interpolated onto the study area with a resolution of 0.25° × 0.25°. The interpolated value at any grid point is based on linear interpolation of the values at neighboring grid points in each respective dimension. The number of the grid points analyzed in this study is 2048 over the study area for both reanalysis data. Moderate winds are represented by $U10_m$ and the severe winds are represented by 95th percentile wind speeds ($U10_{95}$).

2.3. Methodology

To reveal the long-term trends in *U10* over the study area, time series each consisting of 38 values between 1979 and 2016 are constructed for both $U10_m$ and $U10_{95}$. Seasonality of wind and wave climate of the Black Sea has been shown in previous studies (Rusu et al. 2018; Aydogan 2017; Aydogan and Ayat 2018). To analyze the seasonality of the variables, spatiotemporal variations are analyzed for each month separately, as well as the annual variations. Hence we constructed 26 time series (12 monthly time series and one annual time series for both $U10_m$ and $U10_{95}$) each including 38 values at each grid point for ERA-I and CFSR data. We analyzed 53,248 (2048 × 26) time series in total. Analysis results are presented in means of percentages rather than the exact rates of change in *U10*. *U10* values are normalized by each gird's mean value to get the relative trend in each time series as shown in Eq. 1,

$$U10^*_{k,t} = U10_{k,t}/\bar{U}_k, \tag{1}$$

where $U10^*_{k,t}$ is the normalized *U10*, $\bar{U}$ is the mean of *U10* series being calculated, *k* is the grid number and *t* is the time step.

For each time series at each grid point, trends are estimated by using Theil–Sen's estimator and Mann–Kendall test to detect the variations of the $U10_m$ and $U10_{95}$ time series. The Mann–Kendall test, introduced by Kendall (1938, 1970) and Mann (1945), is a non-parametric test that does not require the data to be normally distributed and has low sensitivity to outliers in the time series. The Mann–Kendall test is often combined with the Theil–Sen estimator, which is used to fit a line through the sample points in the coordinate system (simple linear regression) by calculating the median of the slopes of all lines along with the pairs of the data points (Sen 1968).

Mann–Kendall test (Kendall 1938; Mann 1945) is an instrument used to test whether a randomly distributed time series has a monotonic (increasing or decreasing) trend or not. No trend case is defined as a null hypothesis against the alternative hypothesis which means that there is a monotonic trend. The test evaluates the data values and ordered time series and compare each data value with all subsequent ones. If

Table 1

Properties of the reanalysis U10 data used in this study

Reanalysis	Start date	End date	Temporal resolution (h)	Original spatial resolution	The spatial resolution used in this study
ERA-I	01/01/1979	31/12/2016	6	0.7° × 0.7° (∼ 80 km)	0.25° × 0.25° (∼ 27 km)
CFSR	01/01/1979	31/12/2016	6	0.312° × 0.312° (∼ 38 km)	0.25° × 0.25° (∼ 27 km)

a data value is smaller than a later one, a *statistic S is increased by one; on the contrary, S* is decreased by one if a data value is larger than the one at a later period of time. After evaluating all data values, S comes out with a final value (Shadid 2011). If the final value of S is positive, this refers to the existence of an increasing trend; a negative value of S refers to a negative trend. S is calculated using Eq. 2;

$$\operatorname{sgn}(x_j - x_k) = \begin{cases} +1 & if\ x_j - x_k > 0 \\ 0 & if\ x_j - x_k = 0 \\ -1 & if\ x_j - x_k < 0 \end{cases} \quad (2)$$

$$S = \sum_{k=1}^{n-1} \sum_{j=k+1}^{n} sgn(x_j - x_k)$$

where x_j and x_k are the data values in time j and k, respectively ($j > k$), (Gilbert 1987).

To evaluate a trend whether it is significant at α level or not, statistic Z value is used. The null hypothesis is rejected if the$|Z| > Z_{1-\alpha/2}$, where $Z_{1-\alpha/2}$ is obtained from standard normal cumulative distribution tables (Salmi et al. 2002). Z is calculated using Eq. 3;

$$Z = \begin{cases} \frac{S-1}{\sqrt{VAR(S)}} & if\ S > 0 \\ 0 & if\ S = 0 \\ \frac{S+1}{\sqrt{VAR(S)}} & if\ S < 0 \end{cases} \quad (3)$$

$$VAR(S) = \frac{1}{18}\left[n(n-1)(2n+5) - \sum_{p=1}^{q} t_p(t_p-1)(2t_p+5)\right]$$

where q is the number of tied groups and t_p is the number of data values in the pth group (Salmi et al. 2002) (Drapela and Drapelova 2011).

In case of the existence of a linear trend for a time series, a true slope which defines the change per unit time can be evaluated by using Sen's slope estimator (Sen 1968). In Sen's slope nonparametric procedure, the linear model is described in Eq. 4;

$$f(t) = Q_t + B, \quad (4)$$

where Q is the slope and B is a constant.

Q is determined by using each slope of the lines across all data pairs, Q_i (Eq. 5). There are $N = n(n-1)/2$ slope estimates, Q_i, for a time series with n values. The Sen's slope is found to be the median of these N values as shown in Eq. 6 (Drapela and Drapelova 2011),

$$Q_i = \frac{x_j - x_k}{j-k}, i = 1, 2, 3, \ldots, N, j > k \quad (5)$$

$$Q = \begin{cases} Q_{\frac{N+1}{2}} & if\ N\ is\ odd \\ \frac{1}{2}\left(Q_{\frac{N}{2}} + Q_{\frac{N+2}{2}}\right) & if\ N\ is\ even \end{cases} \quad (6)$$

The calculations for the trend analysis of the *U10* data are done by using in house code via the MATLAB© Environment. The results including Sen's Slope and their significance at 95% or higher confidence level are explored and represented by color contours on spatial maps. All maps are created by using Ocean Data View Software (Schlitzer 2019). Also, some key study sites at important coastal zones of the Black Sea (Fig. 1) are analyzed further to study interannual variations in the time series.

3. Results and Discussion

3.1. Comparison of Two Reanalysis U10 Data and Interannual Variability

Comparison of CFSR and ERA-I reanalysis *U10* data is essential to provide an understanding of differences in basic characteristics of two leading data. For this purpose, long-term averages of *U10* over 38 years (1979–2016) are mapped for both ERA-I and CFSR in Fig. 2. Only the magnitudes are considered, wind directions are not analyzed. Grid points based on the native spatial resolution are indicated with dots on spatial maps in Fig. 2. Land/Sea mask data are obtained from ERA-I and CFSR for corresponding reanalysis data and depicted in Fig. 2. In Fig. 2, the land area is indicated by white dots where the sea points are indicated by black dots.

Figure 2 shows that the spatial distribution of long-term averaged of *U10* from two reanalysis data over the Black Sea Basin presents a similar pattern. Higher long-term averaged *U10* values occur in the center of the Sea of Azov and offshore northwestern Black Sea. Where the lowest long-term averaged *U10* values exist in the eastern part of the basin. For the land area, the northern part of the Black Sea has higher long-term averaged *U10* values than the south.

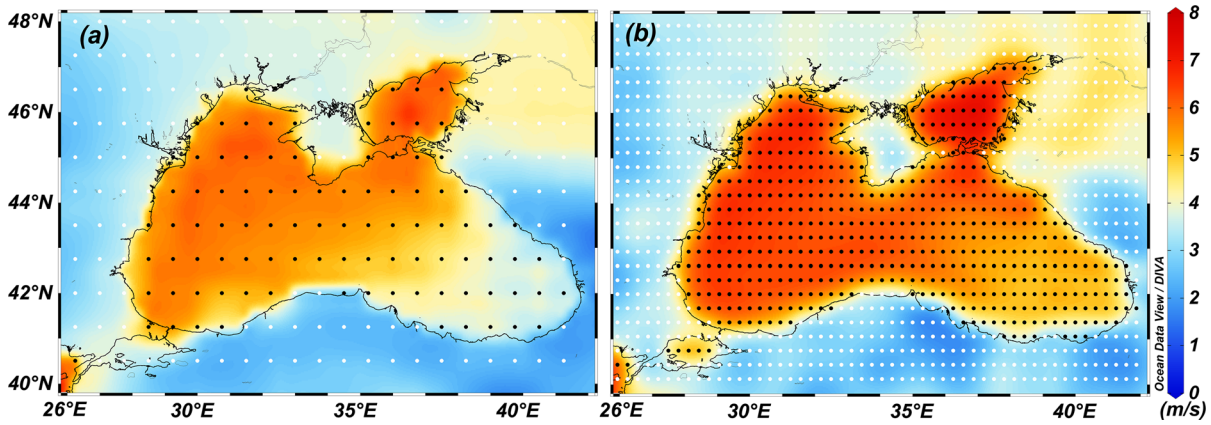

Figure 2
Long-term averaged *U10* considering 38 years period (1979–2016) over the Black Sea: **a** ERA-I, **b** CFSR. White dots indicate land and the black dots indicate sea points

Generally, CFSR gives higher long-term averaged *U10* values in the sea. The Sea of Marmara exhibits much higher long-term averaged *U10* in CFSR data since it is considered as open sea whereas it is considered as a land area in ERA-I data. A clear magnitude difference between the two data is revealed. The long-term averaged *U10* from ERA-I varies between 1.63 and 6.63 m/s with an average value of 4.04 m/s (Fig. 2a). CFSR data varies between 1.74 and 7.35 m/s with an average value of 4.42 m/s (Fig. 2b). To quantify the magnitude difference from both reanalysis data the ratio of CFSR long-term averaged *U10* to ERA-I long-term averaged *U10* is computed spatially as illustrated in Fig. 3.

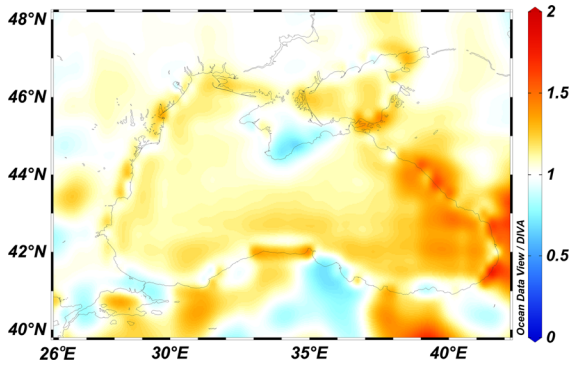

Figure 3
The ratio of long-term average *U10* values from the CFSR data to the ones from ERA-I

Figure 3 presents that, the magnitude of the difference between long-term averaged *U10*s from two data is inhomogeneous throughout the study area. The ratio of long-term averaged *U10* from CFSR to long-term averaged *U10* from ERA-I varies between 0.66 and 1.8 with a basin average value of 1.10. CFSR gives higher long-term averaged *U10* values in most of the study area where the only exceptions are coastlines along the Crimean Peninsula, and southern coasts of the Black Sea basin. Ratios smaller than one occur along the shoreline of the Crimean Peninsula, Strait of Istanbul and Dardanelles. Highest ratios exist along the eastern coasts of the Black Sea, westernmost and southern coasts of the Sea of Azov, and along the eastern Black Sea coastlines. On land area, the highest rates of ratio occur in the eastern part of the study area.

Long-term variations of the *U10* are analyzed for both ERA-I and CFSR reanalysis data, comparatively. We evaluated the annual $U10_m$ and $U10_{95}$ time series for each corresponding grid points during the study period covering 38 years in between 1979 and 2016. In Fig. 4, time series from the selected study sites (Fig. 1) are shown to present the interannual variability in both annual $U10_m$ and $U10_{95}$ over different parts of the Black Sea.

Figure 4 indicates different interannual patterns in the temporal long-term evaluations of moderate and severe *U10* values over the Black Sea. Both reanalysis data presents similar interannual variability for

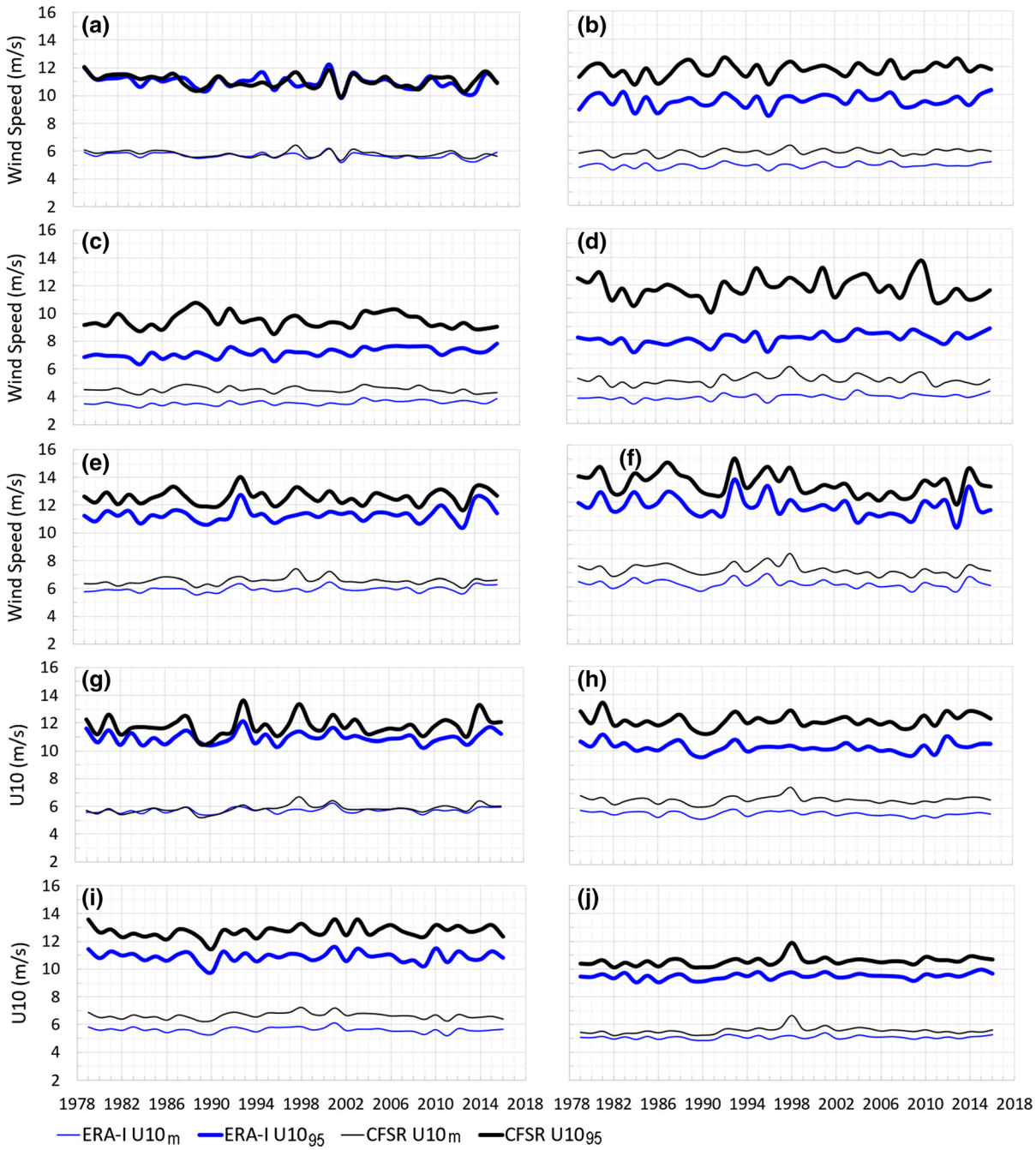

Figure 4
Interannual variability of annual $U10_m$ and annual $U10_{95}$ at selected study sites (Fig. 1), **a** A, **b** B, **c** C, **d** D, **e** E, **f** F, **g** G, **h** H, and **i** I, **j** J

almost all the study sites for both annual $U10_m$ and annual $U10_{95}$. Although the interannual variability looks similar, CFSR data gives higher annual $U10$s at almost all study sites. Higher time-averaged differences between ERA-I and CFSR exist for the annual $U10_{95}$ than the annual $U10_m$ reaching up to 3 m/s in B, D and H. Interannual Variability (IV) is calculated at the selected study sites for both

reanalysis data and both the annual $U10_m$ and annual $U10_{95}$ as shown in Eq. 7,

$$IV = \frac{U10_{\max} - U10_{\min}}{U10_{mean}} \tag{7}$$

IV of Differences (IVD) is computed for the temporal evolution of the differences between ERA-I and CFSR data as shown in Eq. 8,

$$IVD = \frac{(U10_{CFSR} - U10_{ERA-I})_{\max} - (U10_{NCEP} - U10_{ERA-I})_{\min}}{(U10_{ERA-I})_{mean}} \tag{8}$$

Computed IV and IVD values are shown in Table 2.

Table 2 shows that the interannual variability of the annual $U10$ is slightly smaller than the interannual variability of the annual $U10_{95}$ based on the ERA-I data, while they are higher based on the CFSR data. The highest IV computed in D from both reanalysis data. Whereas the smallest variability computed in H from the ERA-I data, and in I from the CFSR data. These highest and lowest IV patterns are found to be consistent with annual $U10_m$ *and* $U10_{95}$ data, but they are inconsistent between two considered reanalysis data. Basin-averaged IV is much smaller with respect to the IVs for the considered study sites for the ERA-I data. It is relatively smaller for the CFSR data as well. IVD presents wider range variability for both annual $U10_m$ and annual $U10_{95}$ over the Black Sea coastline. The highest and lowest IVD for annual $U10_m$ are computed at D and I, respectively. It is also revealed that the variability of differences between two reanalysis data is much higher for the annual $U10_m$ than the annual $U10_{95}$.

Table 2

Interannual variability coefficients for the selected study sites and the basin averaged U10

Study site	IV				IVD	
	ERA-I		CFSR			
	$U10_m$	$U10_{95}$	$U10_m$	$U10_{95}$	$U10_m$	$U10_{95}$
A	0.17	0.22	0.19	0.20	0.15	0.16
B	0.15	0.19	0.16	0.17	0.14	0.16
C	0.20	0.21	0.16	0.24	0.28	0.33
D	0.26	0.21	0.30	0.31	0.35	0.32
E	0.16	0.21	0.21	0.19	0.19	0.11
F	0.20	0.29	0.24	0.24	0.20	0.10
G	0.15	0.17	0.25	0.26	0.20	0.20
H	0.13	0.16	0.21	0.18	0.16	0.11
I	0.16	0.17	0.15	0.17	0.12	0.09
Basin-averaged *U10*	0.11	0.10	0.26	0.17	0.24	0.15

3.2. *Spatial Variations of Long-Term Trends in Annual $U10_m$ and Annual $U10_{95}$*

As it is seen from the interannual variability analysis of $U10$ over 38 years at selected sites, long-term variability is inhomogeneous over the study area. To study the long-term trends and their spatial variability, trends of 38 year-long time series of both annual $U10_m$ and annual $U10_{95}$ are computed at each grid point over the study area at 0.25° × 0.25° resolution. 12,288 (2048×6) time series in total are analyzed and results are presented as maps in this section. Considering that the atmospheric pressures are the forcing causing wind, we analyzed the long-term trends in Mean Sea Level Pressure (MSLP) from both reanalysis data over the same time period (1979–2016) and the same study area. Long-term trends in MSLP, annual $U10_m$, and annual $U10_{95}$ are shown in Fig. 5. Locations with statistically significant trends at 95% or higher confidence level are depicted by black dots. Time-averaged MSLP over 38 years is also shown as contour maps in Fig. 5a and b. All trend estimates are computed and presented as (%/year).

Figure 5 shows that two reanalysis presents different rates of change in pressure fields over the study area. ERA-I indicates a decreasing trend in the MSLP values as shown in Fig. 5a. Especially the changes in eastern and northeastern parts statistically significant at 95% or higher confidence level. No statistically significant increasing trends has been found in both reanalysis data. The most important difference between two reanalysis data manifested itself over the Anatolian Peninsula where CFSR data shows statistically significant increasing trends in Fig. 5b while ERA-I shows no significant trend. Since this increase occurs over land, it can be said that no significant trend exists over the sea grids for CFSR data. Long term mean values of MSLP are consistent between two reanalysis data.

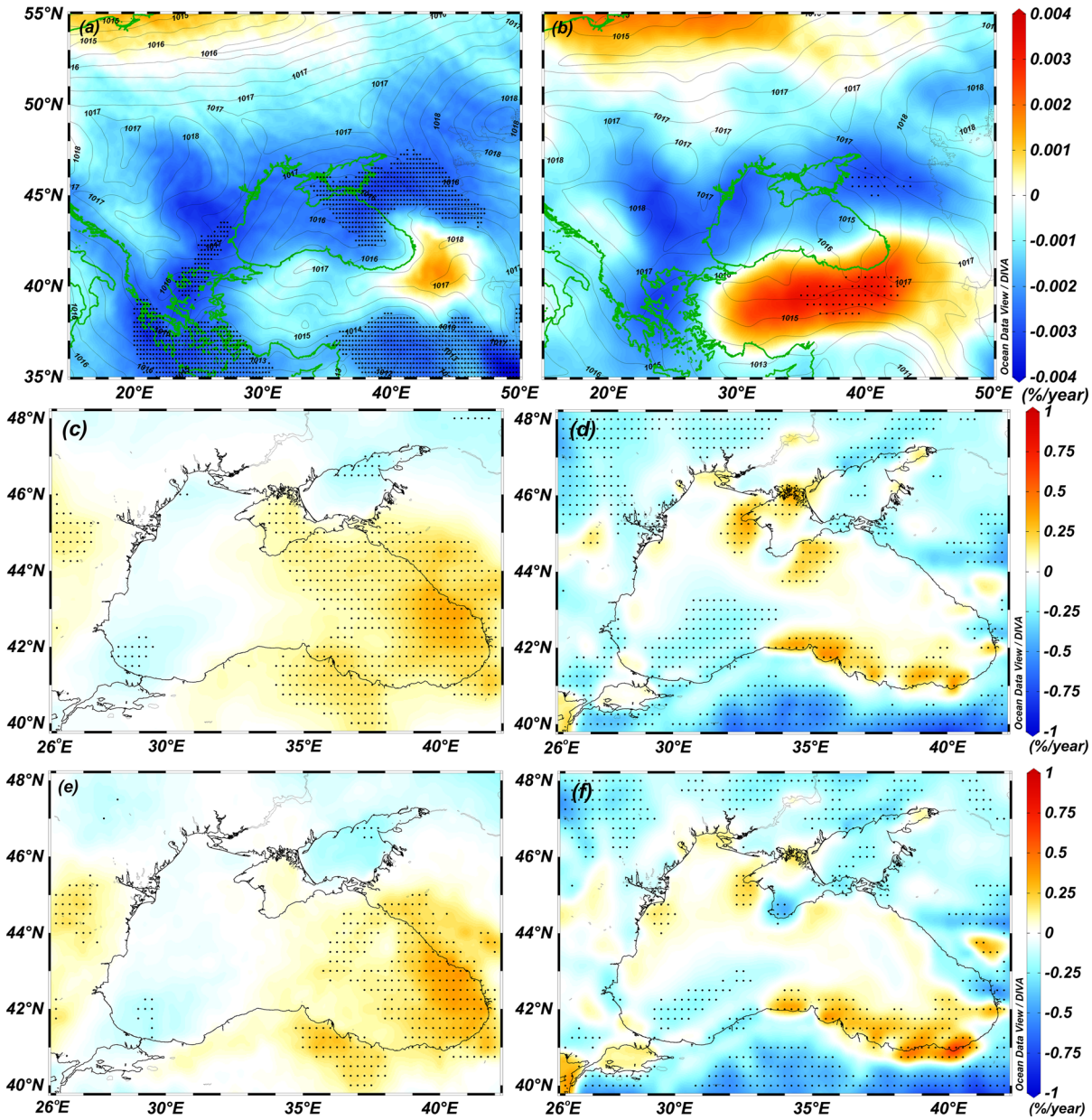

Figure 5
Spatial variability of long-term trends of **a** MSLP from ERA-I, **b** MSLP from CFSR, **c** ERA-I annual $U10_m$, **d** CFSR annual $U10_m$, **e** ERA-I annual $U10_{95}$, **f** CFSR annual $U10_{95}$ for the study period (1979–2016) over the study area. Black dots indicate locations with statistically significant trends at the 95% or higher confidence level. Contours indicate the time-averaged MSLP (Pa) in **a** and **b**

In Fig. 5c and e, ERA-I data shows statistically significant increasing trends in the eastern part of the Black Sea and along the coastline of Kizilirmak and Yesilirmak Deltas for both $U10_m$ and $U10_{95}$. These increasing trends reach the highest rates (0.35%/year) along the Georgia coastline. Statistically significant decreasing trends are computed at the Odessa coastline, southwestern coasts and the Sea of Azov reaching down to − 0.17%/year for annual $U10_m$ from ERA-I. Spatial variation of changes in annual

$U10_{95}$ in Fig. 5e presents statistically significant trends varying between − 0.23%/year and 0.38%/year in the Black Sea basin. Highest and lowest trends are computed along the nearshore Georgia, and the northern coasts of the Sea of Azov, respectively. Comparison of trend rates of annual mean and annual $U10_{95}$ from ERA-I reveals that changes in severe wind states occur at higher rates than the moderate wind states.

Long-term trends computed based on CFSR data slightly higher than the ERA-I for both annual $U10_m$ and annual $U10_{95}$. Trends in annual $U10_m$ varies between − 0.28%/year and 0.41%/year, spatially as depicted by Fig. 5d. Statistically significant decreasing trends exist only the offshore parts of the southwestern Black Sea with rates down to − 0.21%/year. Statistically significant increasing trends occur mostly in the sea area along the Danube Delta coastal zone, the southern and southeastern coastal strip of the Black Sea basin, and along the nearshore and offshore zones of Crimean Peninsula. Statistically significant decreasing trends are computed in the central and northern parts of the Sea of Azov. Highest decreasing trends in annual $U10_m$ computed on the land area, especially at the eastern and southern parts of the study area (Fig. 5d).

Figure 5f presents a similar pattern of spatial variability of long-term trends in annual $U10_{95}$ with the one presented in Fig. 5d. Statistically significant increasing trends manifest themselves over a wider sea area, where statistically significant decreasing trends cover a narrower area. An important difference between Fig. 5d and f exists along the northwestern coasts of the basin where statistically significant increasing trends occur in annual $U10_{95}$. Trends presented in Fig. 5f varies between − 0.41%/year and 0.66%/year, indicating the highest rates of change in a statistically significant increasing trend. The highest trend rate for the increasing $U10_{95}$ is computed to be along the southeastern Turkish coasts of the Black Sea. The highest decreasing trend in Fig. 5f is computed over the continental shelf of Georgia. Figure 5f also indicated statistically significant decreasing trends in the Sea of Azov.

3.3. Spatio-Seasonal Variations of Long-Term Trends in Annual MSLP, Annual $U10_m$ and Annual $U10_{95}$

Seasonal variations are expected in the Black Sea. To illustrate the seasonality in the data, we constructed a time series of mean MSLP, $U10_m$ and $U10_{95}$ on a monthly basis from both reanalysis data. The same temporal coverage of 38 years (1979–2016) is considered for the analysis. Monthly spatial variations of long-term trends in annual MSLP is shown in Fig. 6 for the ERA-I reanalysis data.

It is clear that spatial variability of mean MSLP and the long term trends in MSLP are inhomogeneous and vary seasonally. Influence of Syberian Anticyclone is seen over the eastern basin during winter according to 38-year means. Results indicate that its influence has a significant increasing trend for December. Statistically significant increasing trend rates reaches up to 0.01%/year over the terrestrial part of the easternmost study area. Southeastern part of the study area presents decreasing trends for summer low pressure systems. These statistically significant decreasing trends are computed to be − 0.01%/year. This effect is found for the term from April to September except August where no significant trend exist. The influence of the Mediterranean cyclonic activity is visible for July, August, and September and exhibit statistically significant decreasing trends reaching down to − 0.01%/year.

Monthly spatial variations of long-term trends in annual MSLP is shown in Fig. 7 for the CFSR reanalysis data.

Figure 7 showed that 38-year long term means of MSLP are consistent from both reanalysis for almost all months. Statistically significant decreasing trends in Mediterranean cyclonic activity has also been captured by the CFSR reanalysis data whereas the influence of summer low pressure at the southern part of the study area presents no significant trends. The activity of the Syberian anti-cyclone and increasing trends in its influence has also been captured by CFSR at almost same rates with that of the ERA-I for December.

Monthly spatial variations of long-term trends in annual $U10_m$ is shown in Fig. 8 for the ERA-I reanalysis data.

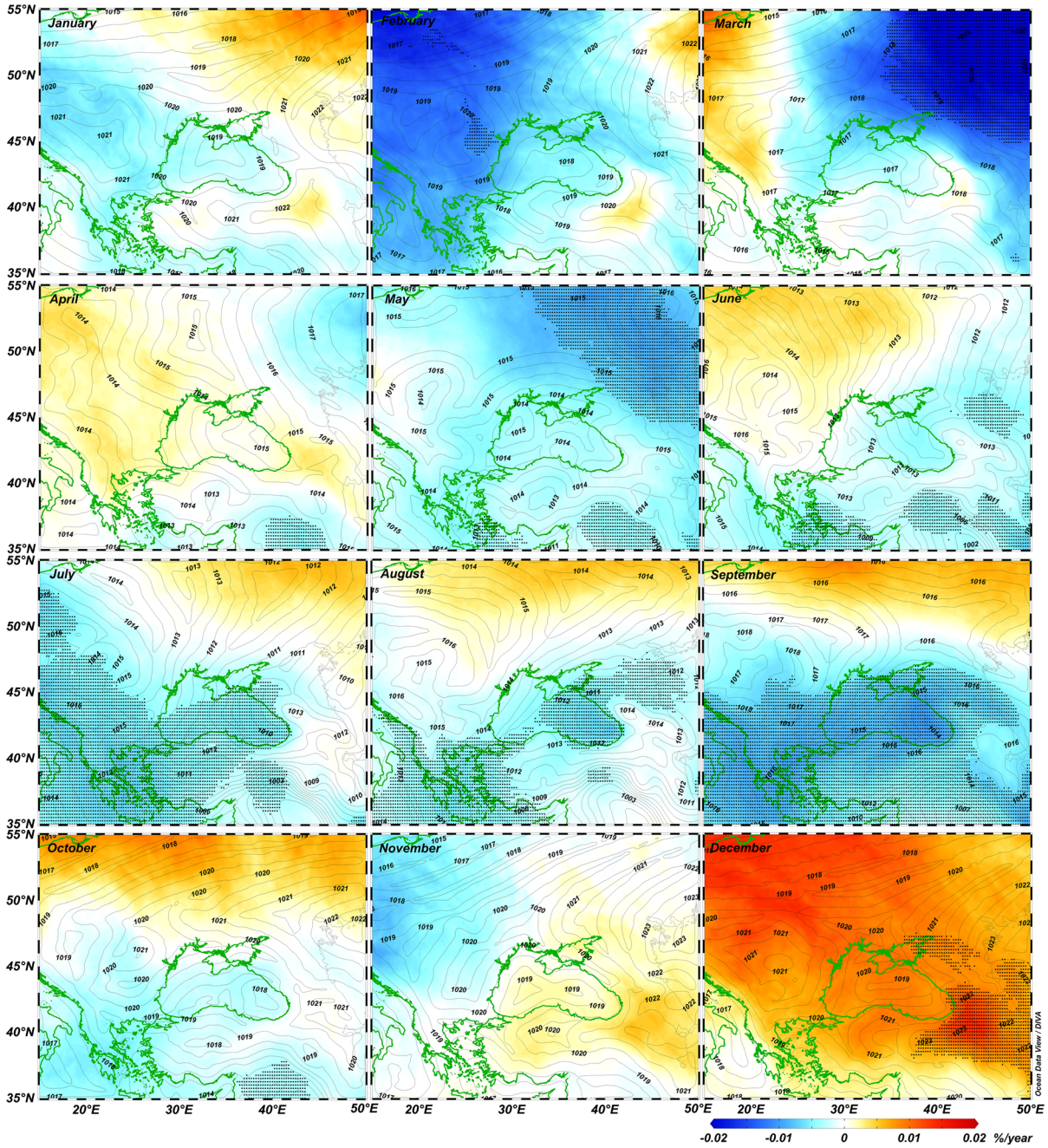

Figure 6
Spatial variability of long-term trends in ERA-I MSLP on a monthly basis. Black dots indicate locations with statistically significant trends at the 95% or higher confidence level

Figure 8 illustrates that the Black Sea manifests clear seasonality in means of long-term trends of monthly $U10_m$ based on ERA-I data. The rates of trends are found to be in between − 0.56%/year (in Sea of Azov for month January) and 0.96%/year (in eastern coasts of the Black Sea for March) over the study area in months January and March, respectively. Highest positive trends are computed in

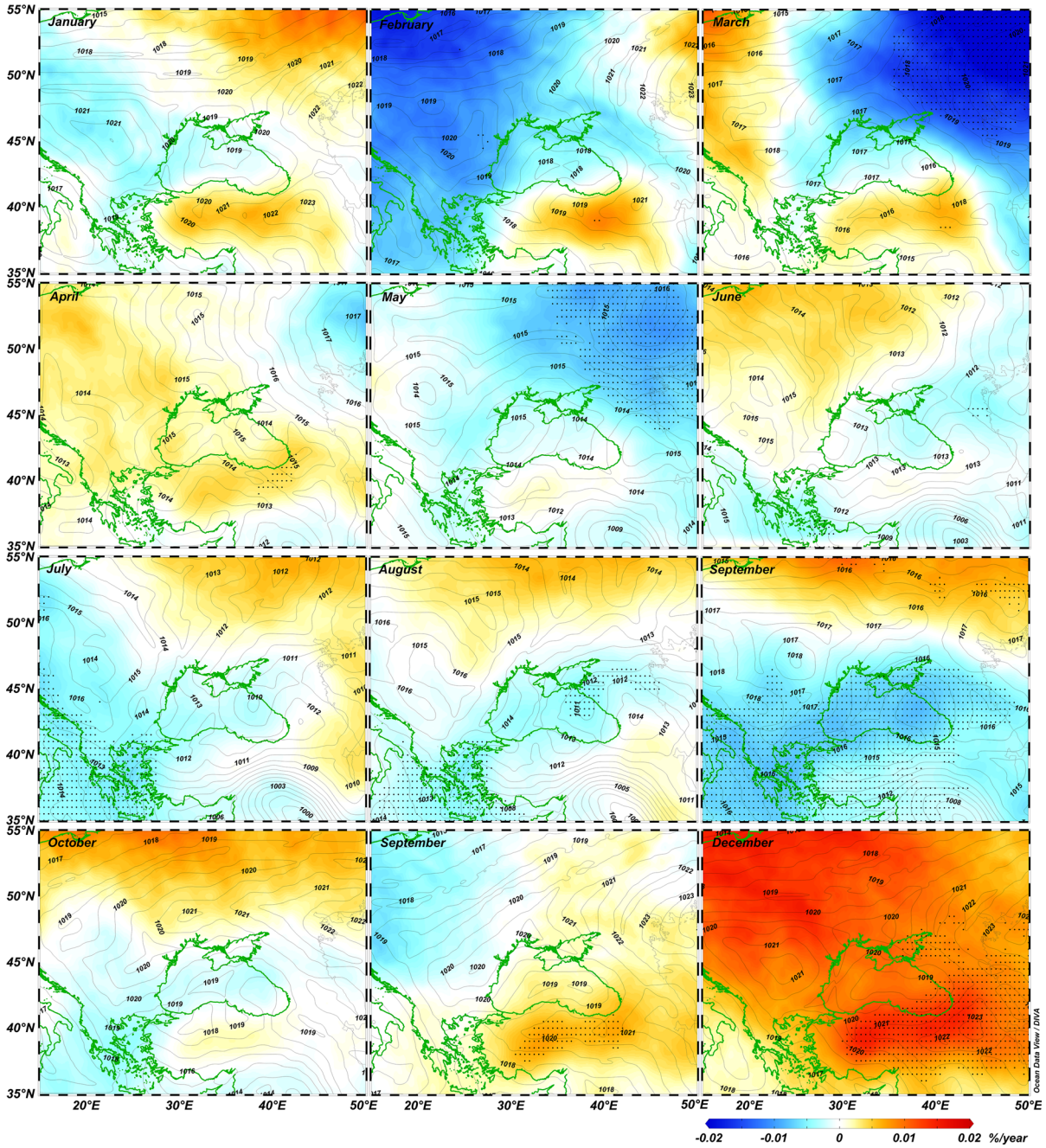

Figure 7
Spatial variability of long-term trends in CFSR MSLP on a monthly basis. Black dots indicate locations with statistically significant trends at the 95% or higher confidence level

February and March along the eastern part of the basin including both the terrestrial and aquatic parts of the coastal zone. January, April, June, October and December also present statistically significant increasing trends at the eastern part of the basin with lower trend rates. The Sea of Azov manifests significantly increasing trends in September and in August partly, where the statistically significant

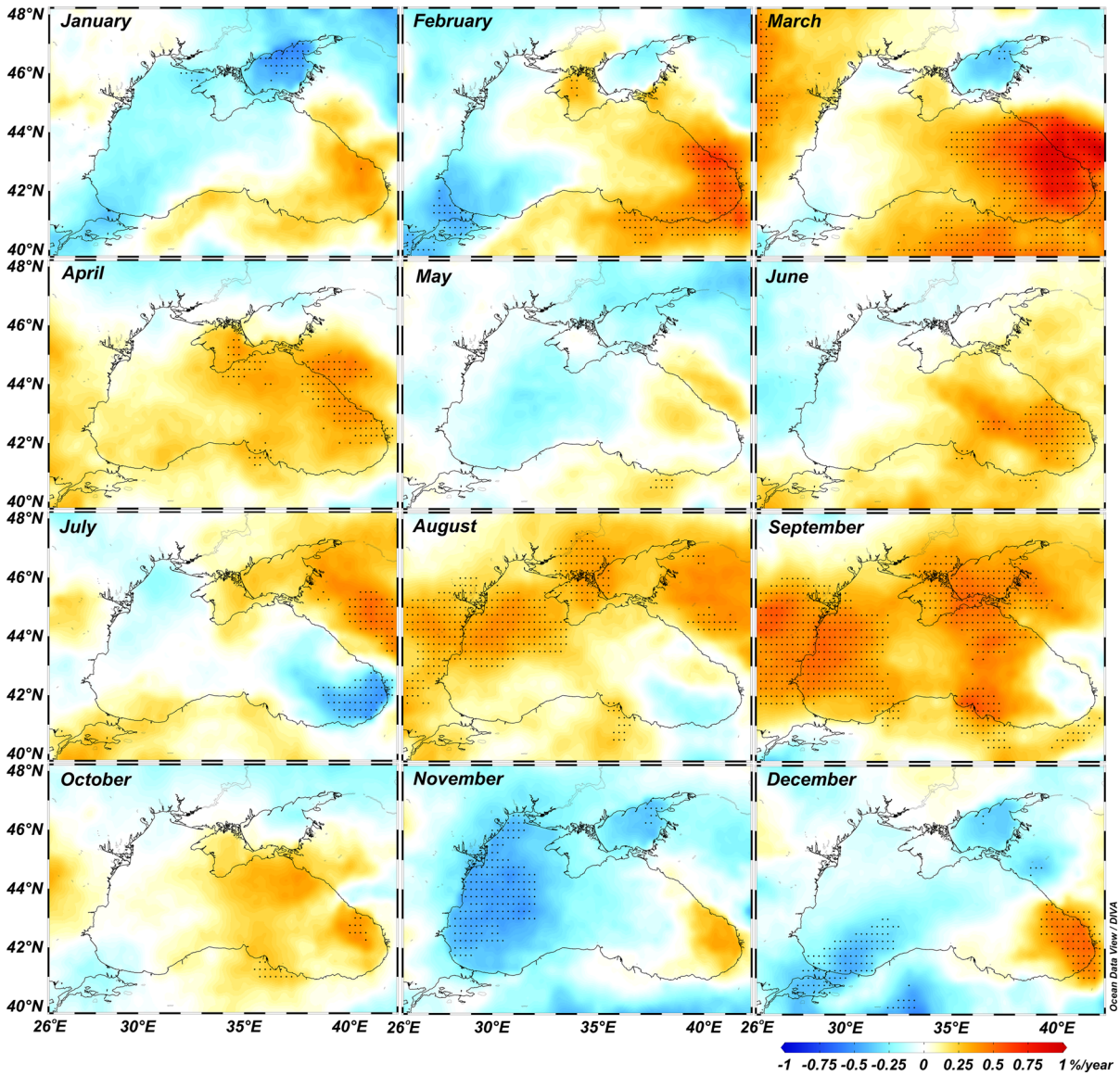

Figure 8
Spatial variability of long-term trends in ERA-I monthly $U10_m$ on a monthly basis. Black dots indicate locations with statistically significant trends at the 95% or higher confidence level

decreasing trends are estimated for January, March, November and December. Other statistically significant decreasing trends are computed along the eastern, western and southwestern coasts of the basin for the months July, November, and December, respectively. No statistically significant decreasing trend is revealed at Crimean Peninsula coastal area while increasing trends are estimated for months April, August, and September. No significant increasing or decreasing trend is found for month May except decreasing trends at the central western part of the basin. By generally saying, $U10_m$ values are found to be increasing at all seasons at the eastern Black Sea, and decreasing trends exist at the transition from summer to autumn (for the months August and September) at the western part. In September

most of the basin together with the Sea of Azov presents a statistically significant increasing trend reaching up to 0.59%/year at Kizilirmak Delta coastline.

Spatial distributions of trends in annual $U10_m$ from CFSR reanalysis data are mapped and presented in Fig. 9.

Figure 9 presents the different spatial distribution of trends in annual $U10_m$ from CFSR reanalysis data. Generally, both decreasing and increasing trends have greater rates than the ERA-I reanalysis data, varying between − 0.62%/year (at southeastern part of the basin for November) and 1.16%/year (at southeastern coasts of the Black Sea for March). Generally increasing trends are covering wider areas

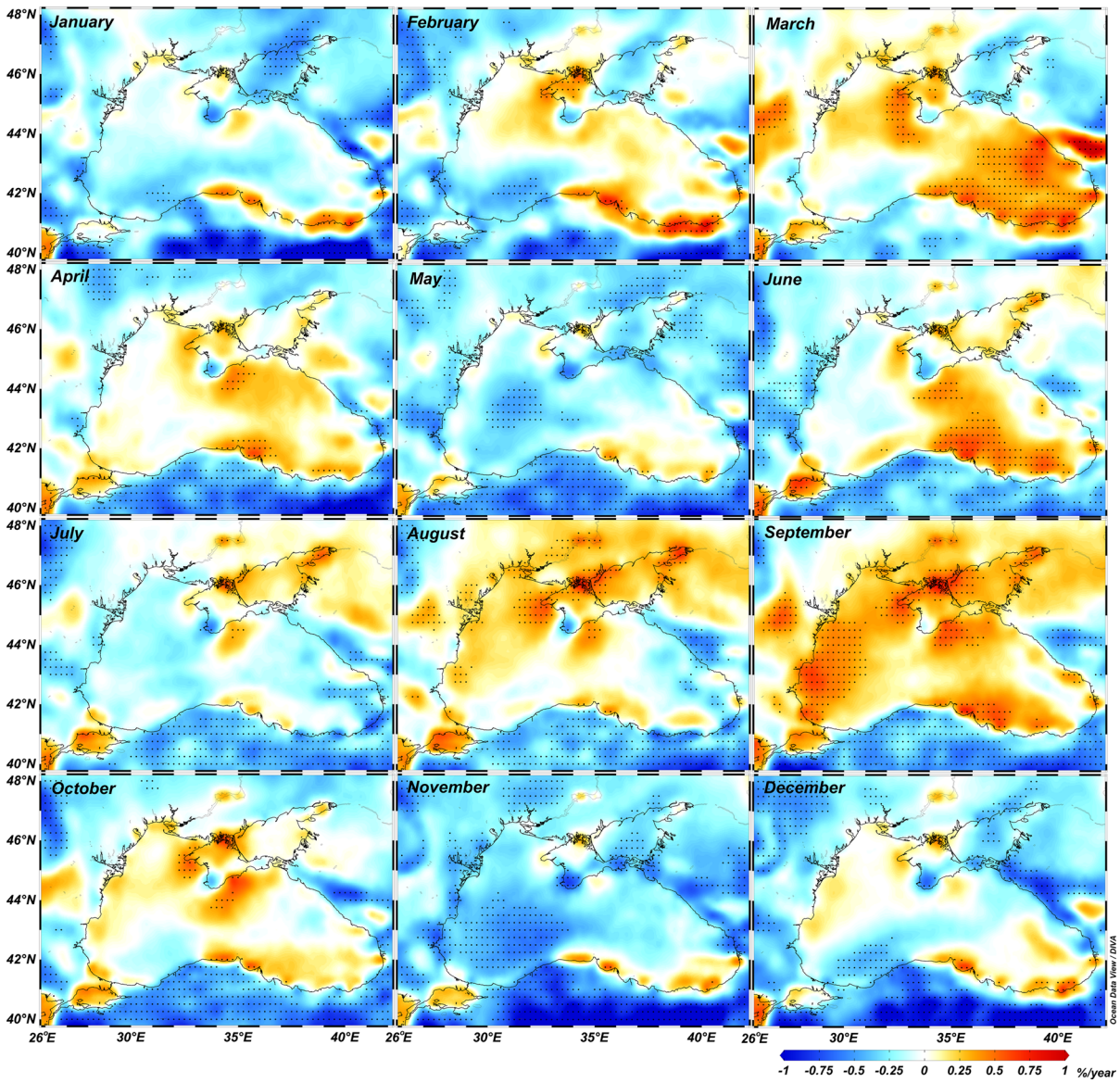

Figure 9
Spatial variability of long-term trends in CFSR monthly $U10_m$ on a monthly basis. Black dots indicate locations with statistically significant trends at the 95% or higher confidence level

existed at greater rates than the statistically significant decreasing trends. Statistically significant increasing trends are computed along the southeastern coasts of the basin for the months March, June, and September. Dramatically varying trends in the terrestrial and aquatic region manifested themselves along the central and southeastern coasts of the Black Sea for all the months. Around the Crimean Peninsula, a consistent statistically significant increasing trends are revealed for months March, April, June, July, August, September, and October. Statistically significant decreasing trends are computed for the months January, May, November, and December in the Sea of Azov where the statistically significant increasing trends are found at a transition from summer to autumn for months August and September.

Understanding the long-term variability in severe *U10s* is also important to evaluate the climate change impacts on the storminess of the Black Sea. Long-term trends in monthly $U10_{95}$ are analyzed on a monthly basis for this purpose. The results are presented in Fig. 10 for the ERA-I reanalysis data.

In Fig. 10, statistically significant decreasing and increasing trends vary between $-$ 0.57%/year and 0.81%/year within the basin for months July and March, respectively. On the land area, the highest increasing trend is computed at the northeastern coasts at a rate of 1.27%/year. Decreasing trends are found for February at northwestern coasts, for March in the Sea of Azov, for May in both sides of Crimean Peninsula, for July along southeastern coasts, and for December in the northeastern part. Statistically significant increasing trends are computed for all months except May and July. Highest statistically significant increasing trends are computed for March, April, and August, along the eastern, northern, and western parts of the basin, respectively. $U10_{95}$ from the ERA-I data are found to be increasing in most of the Black Sea for March, April, and August.

Decreasing trends in the annual $U10_{95}$ in Fig. 10, covers slightly wider area than that of for $U10_m$ in Fig. 8. The coverage of increasing trends is wider for months January, October, and November and narrower for others. While increasing trends manifest themselves in a very limited area at the east with relatively lower rates for January, increasing trends at higher rates exist at the west at the terrestrial zone just behind the coastline.

Spatial distributions of long-term trends in monthly $U10_{95}$ regarding CFSR data is presented in Fig. 11 to provide a comparison between two reanalysis data.

Figure 11 shows statistically significant decreasing and increasing trends varying between -1.50%/year and 1.10%/year over the study area. It is clear that severe winds (represented by monthly $U10_{95}$) present higher increasing/decreasing trend rates with respect to moderate winds (represented by monthly $U10_m$) for each month. Especially the south to southeast coast arc has the highest increasing trend rates followed by the highest decreasing trends behind the coast at the mountainous terrestrial area. This sharp transition between increasing and decreasing trends does not exist in ERA-I data. Another hot location is the Crimean Peninsula characterized by relatively high increasing trends. Comparison of severe (Fig. 11) and moderate (Fig. 9) winds reveals that increasing trends along the south and southeastern coasts are higher for the severe winds than that of the moderate winds while increasing trends for severe winds are lower than that of moderate winds around the Crimean Peninsula for all months except October.

3.4. Statistics of the Spatial Distribution of Trends

To study the size of the area having increasing or decreasing trends for both monthly $U10_m$ and monthly $U10_{95}$ are analyzed statistically for both reanalysis data. Results are presented in Table 3. Only sea points with significant trends are considered.

Table 3 indicates that both $U10_m$ and $U10_{95}$ tend to increase over $\sim$ 36% and $\sim$ 28% of the Black Sea surface area considering annual distribution, respectively. Annual decreasing trends cover a much smaller surface area between $\sim$ 4 and $\sim$ 2% of the Black Sea surface area based on ERA-I reanalysis data. Surface area covered by significant trends (decreasing or increasing) is larger for ERA-I than that of CFSR for annual $U10_m$. Area covered by significant decreasing or increasing annual trends for CFSR narrower with respect to ERA-I for both $U10_m$ and $U10_{95}$. Regarding the ERA-I, almost no

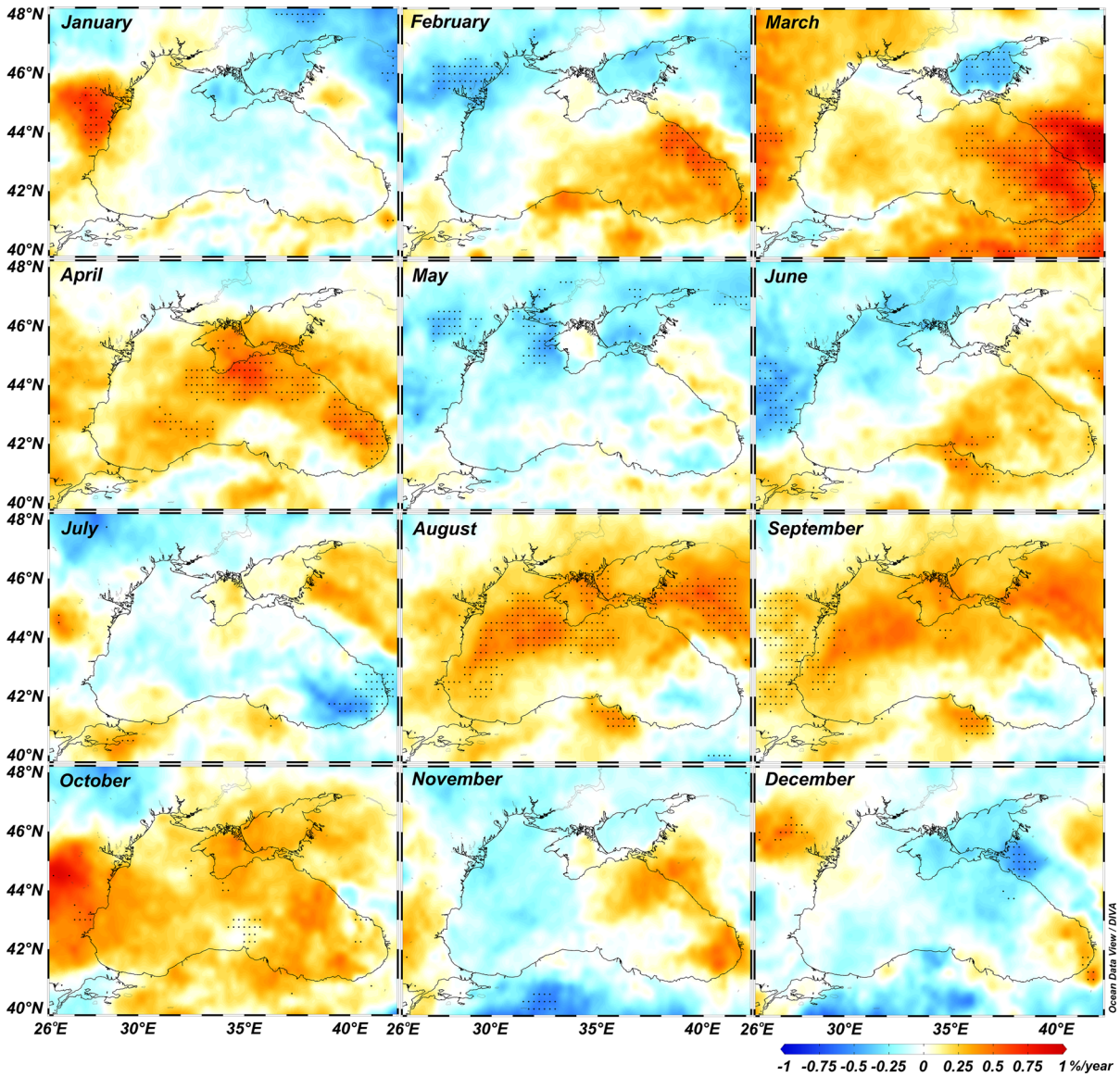

Figure 10
Spatial variability of long-term trends in ERA-I monthly $U10_{95}$ on a monthly basis. Black dots indicate locations with statistically significant trends at the 95% or higher confidence level

decreasing trend in $U10_{95}$ is visible for almost all months and annual computations. In general, increasing trends cover wider surface are for $U10_m$ than $U10_{95}$ if they exist. But significantly increasing trends exist for only 6 months for $U10_m$ whereas they exist for 8 months for $U10_{95}$ based on ERA-I data. Statistically significant decreasing trends exist over less coverage area than the statistically significant increasing trends.

Overall the spatial variability of the long-term trends for both $U10_m$ and $U10_{95}$ in the CFSR data is found to be greater with respect to ERA-I data during the analysis especially along the coastlines. We analyzed time series data for inspecting the reason for the results. Our analysis indicated that the change

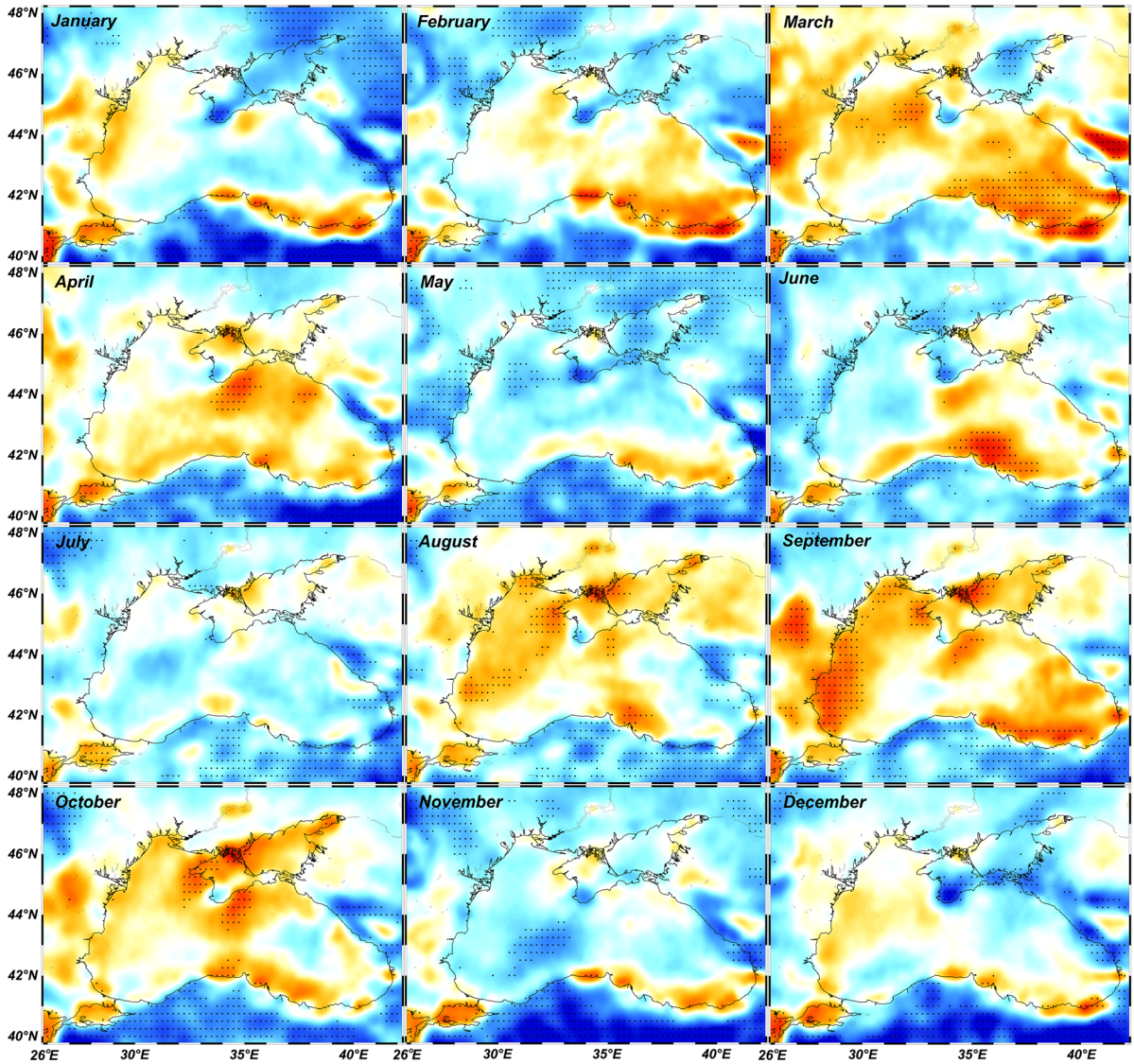

Figure 11
Spatial variability of long-term trends in CFSR monthly $U10_{95}$ on a monthly basis. Black dots indicate locations with statistically significant trends at the 95% or higher confidence level

in the model land/sea mask data during the transition from CFSR version 1 to version 2 created some disturbances in the wind speeds. This effect can be seen in Fig. 4c and d where the wind speeds presents a sudden change after 2011 which is the transition year between the two versions of the models. The clearest effect is visible over the Crimean Peninsula where data indicated a decreasing trend at the center of increasing trends. Although general consistency in between ERA-I and CFSR wind reanalysis data is found in means of the spatial variability of the increasing and decreasing trends, this possible effect of transition from CFSR version 1 and CFSR version 2 must be considered for the significance of the trends and the rates of trends.

3.5. *Relation of Long-Term Variability of U10 to the Teleconnection Patterns*

It has also been a common fact that the wind climate at any location on the earth is related to the wind climate at other locations far away. The

Table 3

Percentage of grid points where statistically significant negative and positive trends exist in monthly/annual $U10_m$ and $U10_{95}$ over the Black Sea

	ERA-I				CFSR			
	(−) Trends in $U10_m$	(+) Trends in $U10_m$	(−) Trends in $U10_{95}$	(+) Trends in $U10_{95}$	(−) Trends in $U10_m$	(+) Trends in $U10_m$	(−) Trends in $U10_{95}$	(+) Trends in $U10_{95}$
January	4.86	0.12	0	0	4.50	1.20	2.14	2.37
February	0	10.79	7.00	0.59	3.60	2.73	0.24	2.49
March	0.59	29.18	3.91	22.18	0.50	26.3	1.90	18.86
April	0	11.63	0	25.15	0	4.74	1.07	4.74
May	0	0	4.39	0	8.10	0.80	7.24	0.47
June	0	11.63	0	1.30	0	15.54	1.42	6.52
July	7.47	0	4.98	0	3.80	1.07	3.32	0
August	0	0	0	7.47	2.80	8.78	3.44	13.88
September	0	0	0	5.46	0	27.60	0	19.34
October	0	0	0	3.68	0	3.70	0	7.59
November	21.47	0	0	0	23.30	0.50	6.64	0.47
December	9.13	6.64	0.47	0.59	7.10	1.80	4.03	1.30
Annual	3.91	36.42	1.78	28.00	15	12.5	8.90	14.47

distances between these two locations are generally huge and sometimes half way around the Earth. The linkage between the variations in dynamic climate variables at a region and the fluctuations of a climate variable such as wind at a remote location described as teleconnection. Teleconnection patterns link weather patterns over large distances across the globe. Atmospheric teleconnections may have an influence on mean and extreme climate parameters (temperature, precipitation or wind) on the global or regional scales and have been used in previous research, widely (Hasanean 2005). The prominent teleconnection patterns over the North Atlantic and their affected regions are; *NAO, EA, EA/WR*, West Pacific (*WP*), East Pacific/North Pacific (*EP/NP*), Pacific/North American (*PNA*), Scandinavia (*SCA*), Tropical/Northern Hemisphere (TNH), Polar/Eurasia (*POL*), Pacific Transition (PT).

In this study, the relationship between long-term variations of *U10* over the Black Sea and teleconnection patterns are also studied. In order to understand the most influencing teleconnection pattern on the temporal variation of the wind fields of the Black Sea, correlation coefficients between each corresponding teleconnection with the $U10_m$ and $U10_{95}$ are computed for *EA* (Wallace and Gutzler 1981), *EA/WR* (Barnston and Livezey 1987), *NAO* (Barnston and Livezey 1987), *PNA* (Barnston and Livezey 1987), *POL* (CPC 2011), and *SCA* (Barnston and Livezey 1987). Only the simultaneous correlations with no lags are studied. Spatial distribution of the Pearson's correlation coefficients (r) between the considered teleconnection patterns and the annual $U10_m$ and annual $U10_{95}$ time series during the study period of 38 years (1979–2016) are presented in Fig. 12. For the 38 years-long time series treshold value of r is 0.304 at a 95% confidence level. Only r values greater than $|\pm 0.304|$ are presented since they are statistically significant in this analysis.

Figure 12 shows that fluctuations in $U10_m$ correlate all the considered teleconnection patterns more or less. PNA correlates with the $U10_m$ from ERA-I positively over the whole basin with r values over 0.4. *EA/WR, NAO*, and *POL* are inversely correlated with the $U10_m$ based on ERA-I along southern, southeastern coasts, and nearby the Crimean Peninsula with r values over 0.5. In the Sea of Azov, dominating teleconnection pattern is SCA for both reanalysis data with r values reaching up to 0.5 for both ERA-I and CFSR data. CFSR data shows that the least influencing teleconnection pattern is *EA/WR* and its influence exist only along the south to southeastern coasts inversely with r values reaching 0.3. POL also has an influence along the southern part of the basin with inverse r values up to 0.5 and 0.4 for CFSR and ERA-I, respectively. The highest r values are reached over 0.6 along the south to southeastern coast by the *EA* based on the CFSR data. *NAO*

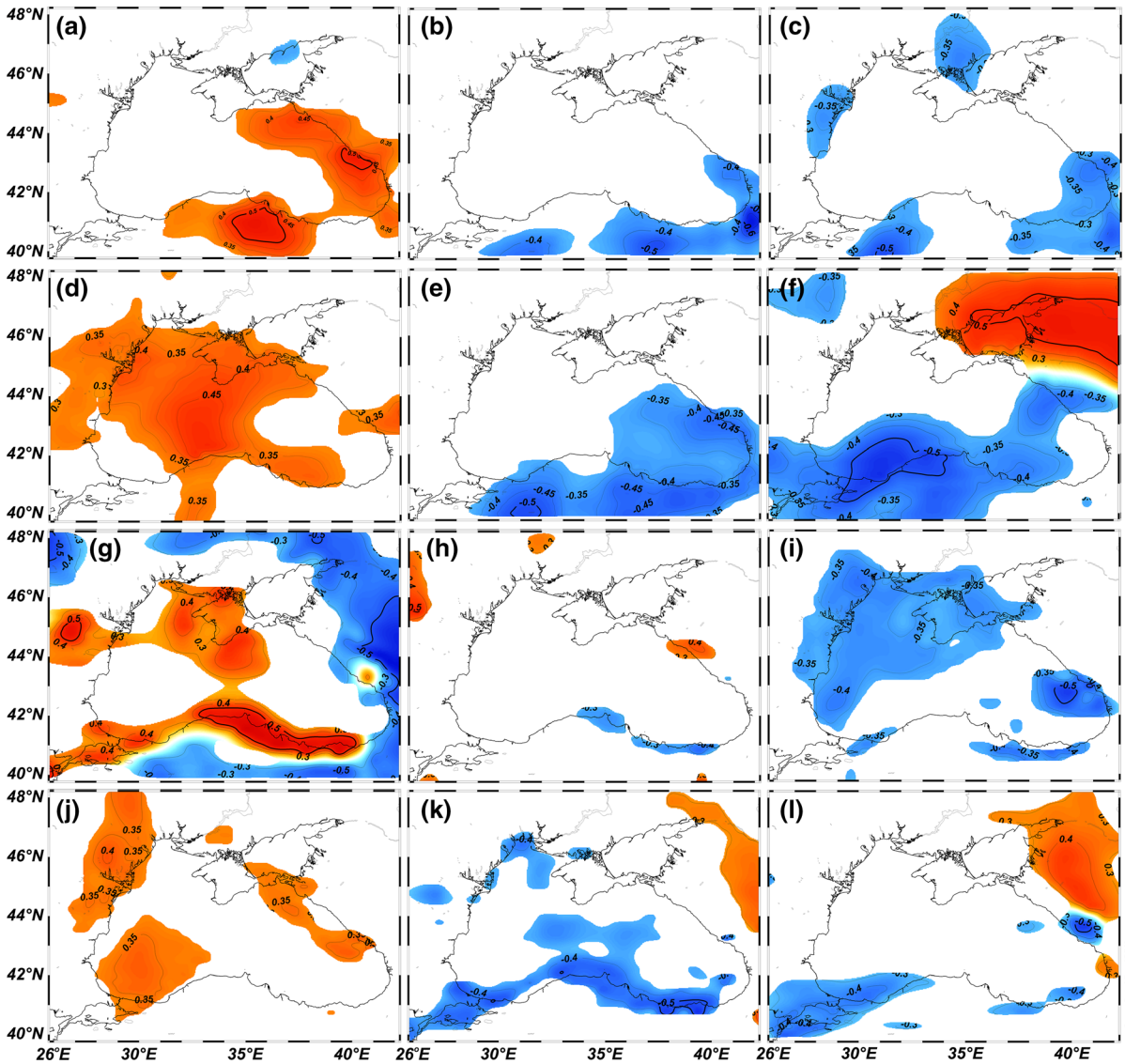

Figure 12
Correlation coefficients between teleconnection indices and the annual $U10_m$ over the Black Sea for both ERA-I and CFSR reanalysis data, **a** [ERA-I]–[*EA*], **b** [ERA-I]–[*EA/WR*], **c** [ERA-I]–[*NAO*], **d** [ERA-I]–[*PNA*], **e** [ERA-I]–[*POL*], **f** [ERA-I]–[*SCA*], **g** [CFSR]–[*EA*], **h** [CFSR]–[*EA/WR*], **i** [CFSR]–[*NAO*], **j** [CFSR]–[*PNA*], **k** [CFSR]–[*POL*], **l** [CFSR]–[*SCA*]

manifests its influence over a wide surface area covering north and northwestern parts of the basin with r values over 0.4 for the CFSR data. In general, CFSR and ERA-I reanalysis data provide consistent spatial distribution patterns and rates of r values over the Black Sea indicating the influence of different teleconnection indices.

It is expected that the severe wind speeds represented by $U10_{95}$ may present different distribution. Spatial variability of the r values between corresponding teleconnection indices and the $U10_{95}$ is presented in Fig. 13 for both ERA-I and CFSR reanalysis data.

Figure 13 indicates that PNA is the most influential teleconnection index over the whole basin with r values reaching over 0.5 and 0.4 at the central Black Sea for both ERA-I and CFSR. For both ERA-I and CFSR data, *EA* has strong influence along the

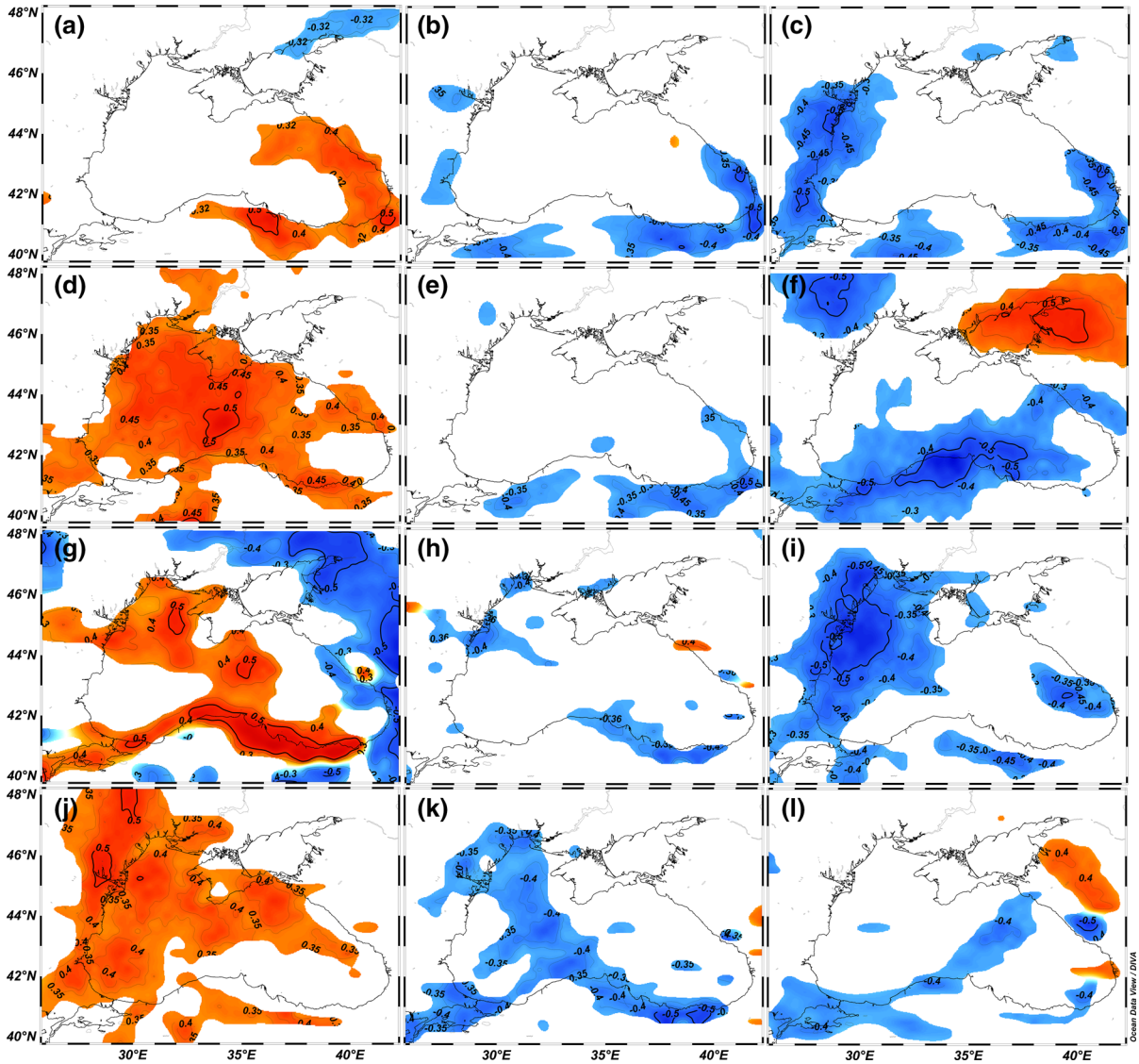

Figure 13
Correlation coefficients between teleconnection patterns and the $U10_{95}$ over the Black Sea for both ERA-I and CFSR reanalysis data. **a** [ERA-I]–[*EA*], **b** [ERA-I]–[*EA/WR*], **c** [ERA-I]–[*NAO*], **d** [ERA-I]–[*PNA*], **e** [ERA-I]–[*POL*], **f** [ERA-I]–[*SCA*], **g** [CFSR]–[*EA*], **h** [CFSR]–[*EA/WR*], **i** [CFSR]–[*NAO*], **j** [CFSR]–[*PNA*], **k** [CFSR]–[*POL*], **l** [CFSR]–[*SCA*]

southeastern coasts with *r* values reaching up to 0.6 at deltaic coasts in the region. The influences of *EA/WR, NAO* and *POL* along the southeastern and eastern coasts are also confirmed by both reanalysis with inverse *r* values over the 0.4. $U10_{95}$ well correlated with *NAO* inversely along the western coasts with *r* values up to 0.6 based on both reanalysis data. Spatial distribution of the *r* values between corresponding teleconnection indices and the $U10_{95}$ presented in Fig. 13 is found to be similar in general with that of $U10_{m}$ (Fig. 10) for both ERA-I and CFSR reanalysis data. The least effective teleconnection index is found to be *EA/WR* with almost no significant correlation over the sea from both ERA-I and CFSR.

3.6. Comparison with the Previous Research

Studying the long-term trends in $U10_m$ and $U10_{95}$ over the Black Sea by using both ERA-I and CFSR

data enhanced the understanding of how these two major reanalysis data differ from each other. The inter-comparison of two reanalysis data is also the focus of some other researchers. Stopa and Cheung (2014) compared wind speeds from ERA-I and CFSR by using the same set of buoy observations from several locations over the global oceans. They concluded that both data provide a reasonably good match with the buoy and altimetry observations. But ERA-I slightly underestimates and the CFSR slightly overestimates the measurements. Although no observational wind data used in this study, our findings confirmed Stopa and Cheung (2014) for the Black Sea by showing that CFSR gives approximately 10% higher long-term average wind speeds than ERA-I over the Black Sea.

Results of the analysis of the long-term averaged *U10* over the Black Sea from CFSR indicated that the highest values exist in Sea of Azov and the north-western offshore parts of the basin. This finding is found to be consistent with the results presented by Rusu et al. (2018). The magnitude of the highest long-term *U10* is estimated as 7.35 m/s in this study where it is reported to be 7.29 m/s in Rusu et al. (2018). Slight differences caused by the analysis of different terms. Rusu et al. (2018) studied 23 year data (1987–2009) whereas it is extended to 38 years (1979–2016) in the present study. Ganea et al. (2019) reported statistically significant decreasing trend with a rate of − 0.01 cm/decade for annual $U10_m$ at the offshore western Black Sea by analyzing ERA-I reanalysis data between 1983 and 2017 whereas our findings indicate no significant trend.

The findings presented in this study are in line with the long-term variations of annual *U10* at selected locations over the Black Sea presented by Akpinar and Bingolbali (2016) based on CFSR reanalysis data for 31 years between 1979 and 2009. It is explored that the annual $U10_m$ over the coasts of the Crimean Peninsula represents a significant increasing trend as 1.33 cm/s/year in the study period (Akpinar and Bingolbali 2016). In the present study, *U10* on the same location shows a significant increasing trend as 1.41 cm/s/year for the term between 1979 and 2016. Besides the authors reported an increasing trend of 0.71 cm/s/year for the south-eastern coasts of the Black Sea, where it is in par with the ones illustrated in the present study as 0.74 cm/s/year. Severe wind states represented by annual maximum wind speeds were also investigated by Akpinar and Bingolbali (2016), however, it is not possible to make a direct comparison between them and the results of the present study in which the $U10_{95}$ are evaluated.

Zainescu et al. (2017) studied the storm variability along the north-western coasts of the Black Sea since 1949 and evaluated the influence of different teleconnection indices. Authors reported a statistically significant correlation of − 0.76 between the *NAO* and the storm variability at Danube Delta coast which is confirmed by our findings in this study for the partly different time period between 1979 and 2016 giving r values of − 0.6.

Although the findings of this study well in line with the previous studies, some slight differences exist due to the different temporal coverages of the studies and consideration of different representive variable ($U10_{\max}$, $U10_{95}$ or some specific definition of sea storms combining wind and wave properties).

4. Conclusions

The long-term trends in both mean and severe wind states over the Black Sea are investigated by comparing two well-established reanalysis data; ERA-I and CFSR. Severe wind states are represented by $U10_{95}$. The relation of the Black Sea wind climate to the known teleconnection indices is also studied. The main findings of this study are summarized below:

1. Long-term trends of the wind speeds show considerable spatial and seasonal variability. In general, both $U10_m$ and $U10_{95}$ have been increasing over the eastern part of the Black Sea. This points out that the Black Sea is inhomogeneous in means of long-term trends in wind speeds. This inhomogeneity must be taken into account in site specific studies instead of using basin averaged quantities.
2. $U10_m$ and $U10_{95}$ show quite similar spatial distributions of trends for both ERA-I and CFSR. But some inconsistencies are revealed between

ERA-I and CFSR in means of the spatial distribution, rates and significance of the trends, especially along the coastline. Our analysis showed that this is occurred due to some local inconsistencies in the land/sea mask data from CFSR version 1 and version 2 models. This feature of CFSR wind data must be considered in use of wind speed time series covering the transition year 2011.

3. ERA-I reanalysis data indicates that moderate and severe wind speeds are increasing over 36% and 28% of the Black Sea surface area, respectively, while they are decreasing over 4% and 2% of the surface area, respectively by considering only sea surface area.
4. ERA-I data indicates that annual $U10_m$ and $U10_{95}$ have statistically significant decreasing trends down to − 0.17%/year and − 0.20%/year in the Sea of Azov, while they have an increasing trend up to 0.35%/year and 0.38%/year in the eastern part, respectively. This result show that severe wind speeds change at higher rates.
5. Long-term trends are shown to have strong seasonality in the Black Sea. The monthly analysis revealed different magnitude increasing or decreasing trends in both monthly $U10_m$ and $U10_{95}$. ERA-I gives the highest increasing trends along the eastern coast with a rate of 0.81%/year in month March and along the western coast with a rate of 0.53%/year in month September for the monthly $U10_m$. For the severe wind conditions, the highest increasing trends are estimated southeastern coast with a rate of 0.68%/year for March and around the Crimean Peninsula with a rate of 0.42%/year for April.
6. Analysis of correlation coefficients between well-known teleconnection indices and the wind speeds revealed that *EA, EA/WR, NAO, PNA, POL*, and *SCA* indices have an influence at different levels and inhomogeneously over the Black Sea. *PNA* has an influence almost all over the basin with statistically significant correlation coefficients over 0.4. *NAO* dominates over the western basin for $U10_m$ and much wider area covering the southwestern, western and northern Black Sea with invers correlation coefficients reaching over 0.4. Southern coasts are dominated by *EA/WR* and POL for both $U10_m$ and $U10_{95}$. Although general consistency is found between ERA-I and CFSR especially in means of the correlation coefficients, slight differences are observed in the spatial distribution and coverage area of each considered teleconnection index among the two reanalysis data.
7. The findings of this study are generally found to be compatible with the existing literature in means of long-term trends of wind speeds and the influence of teleconnection indices over the Black Sea.

Acknowledgements

This study is funded by the Scientific and Technological Research Council of Turkey, TUBITAK (Grant Number: 116M061) and European Union Era.Net RusPlus (Grant Number: BS STEMA 42/2016). Authors thank the European Centre for Medium-Range Weather Forecasts (ECMWF) for providing ERA-Interim wind data, National Oceanic and Atmospheric Administration (NOAA) National Weather Service for providing CFSR wind data, and the EMODnet Bathymetry Portal for shoreline data.

Author contributions All authors contributed to the study conception and design. Material preparation, data collection and analysis were performed by Tunay Çarpar, Berna Ayat and Burak Aydoğan. The first draft of the manuscript was written by Tunay Carpar and all authors commented on previous versions of the manuscript. All authors read and approved the final manuscript.

References

Akpinar, A., & Bingolbali, B. (2016). Long-term variations of wind and wave conditions in the coastal regions of the Black Sea. *Natural Hazards, 84*(1), 69–92. https://doi.org/10.1007/s11069-016-2407-9.

Arkhipkin, V. S., Gippius, F. N., Koltermann, K. P., & Surkova, G. V. (2014). Wind waves in the Black Sea: results of a hindcast study. *Natural Hazards and Earth Systems Sciences, 14,* 2883–2897.

Athanasatos, S., Michaelides, S., & Papadakis, M. (2014). Identification of weather trends for use as a component of risk management for port operations. *Natural Hazards, 72,* 41–61. https://doi.org/10.1007/s11069-012-0491-z.

Aydoğan, B. (2017). Offshore wind power atlas of the Black Sea region. *Journal of Renewable and Sustainable Energy, 9,* 013305. https://doi.org/10.1063/1.4976968.

Aydoğan, B., & Ayat, B. (2018). Spatial variability of long-term trends of significant wave heights in the Black Sea. *Applied Ocean Research, 79,* 20–35. https://doi.org/10.1016/j.apor.2018.07.001.

Barnston, A. G., & Livezey, R. E. (1987). Classification, seasonality and persistence of low-frequency atmospheric circulation patterns. *Monthly Weather Review, 115,* 1083–1126.

Cakiroglu, A. M., Cevher, N. C., & Agirbas, E. (2017). The meteorological Investigation of Turkish coasts of the Black Sea. *Journal of Anatolian Environmental and Animal Sciences, 2*(3), 53–58.

Climate Prediction Center (CPC). (2011). Northern hemisphere teleconnection patterns. (http://www.cpc.ncep.noaa.gov/data/teledoc/telecontents.html)

Dee, D. P., Uppala, S. M., Simmons, A. J., Berrisford, P., Poli, P., Kobayashi, S., et al. (2011). The ERA-interim reanalysis: configuration and performance of the data assimilation system. *Quarterly Journal of the Royal Meteorological Society, 137,* 553–597. https://doi.org/10.1002/qj.828.

Drapela, K., & Drapelova, I. (2011). Application of Mann-Kendall test and the Sen's slope estimates for trend detection in deposition data from Bílý Kříž (Beskydy Mts., the Czech Republic) 1997–2010. *Mendelova Univerzita v Brně, Beskydy, 4,* 133–146.

Dyer, A. J. (1974). A review of flux-profile relationships. *Boundary Layer Meteorology, 7,* 363–372.

Efimov, V. V., & Anisimov, A. E. (2011). Climatic Parameters of Wind Field Variability in the Black Sea Region: numerical Reanalysis of Regional Atmospheric Circulation. *Izvestiya, Atmospheric and Oceanic Physics, 47*(3), 350–361.

Ganea, D., Mereuta, E., & Rusu, L. (2018). Estimation of the near future wind power potential in the Black Sea. *Energies*. https://doi.org/10.3390/en11113198.

Ganea, D., Mereuta, E., & Rusu, E. (2019). An evaluation of the wind and wave dynamics along the European coasts. *Marine Science and Engineering*. https://doi.org/10.3390/jmse7020043.

Georgopoulou, E., Mirasgedis, S., Sarafidis, Y., et al. (2018). Climatic preferences for beach tourism: an empirical study on Greek islands. *Theoretical and Applied Climatology*. https://doi.org/10.1007/s00704-018-2612-4.

Gilbert, R. O. (1987). *Statistical methods for environmental pollution monitoring*. New York: Van Nostrand Reinhold Company Inc.

Hasanean, H. M. (2005). Variability of teleconnections between the Atlantic subtropical high and the Indian monsoon low and related impacts on summer temperature over Egypt. *Atmospheric Science Letters, 6,* 176–182. https://doi.org/10.1002/asl.113.

Healy, T. R. (2018). Coastal wind effects. In C. Finkl & C. Makowski (Eds.), *Encyclopedia of coastal science. Encyclopedia of earth sciences series*. New York: Springer.

Holtslag, A. A. M., & Bruin, H. A. R. (1988). Applied modeling of the nighttime surface energy balance over land. *Journal of Applied Meteorology, 27,* 689–704.

Jiang, Y., Luo, Y., Zhao, Z., & Tao, S. (2010). Changes in wind speed over China during 1956–2004. *Theoretical and Applied Climatology, 99,* 421–430. https://doi.org/10.1007/s00704-009-0152-7.

Kendall, M. G. (1938). A new measure of rank correlation. *Biometrika, 30*(1–2), 81–93.

Kendall, M. G. (1970). *Rank correlation methods* (4th ed.). London: Griffin.

Kostianoy, A. G., & Kosarev, A. N. (2008). *The Black Sea environment*. Berlin Heidelberg: Springer.

Kubryakov, A., Stanichny, S., Shokurov, M., & Garmashov, A. (2019). Wind velocity and wind curl variability over the Black Sea from QuikScat and ASCAT satellite measurements. *Remote Sensing of Environment, 224,* 236–258. https://doi.org/10.1016/j.rse.2019.01.034.

Li, Z., Yan, Z., Tu, K., Liu, W., & Wang, Y. (2011). Changes in wind speed and extremes in Beijing during 1960–2008 based on homogenized observations. *Advances in Atmospheric Sciences, 28*(2), 408–420. https://doi.org/10.1007/s00376-010-0018-z.

Mann, H. B. (1945). Nonparametric tests against trend. *Econometrica, 13*(3), 245–259.

Masuda, D., Kai, S., Yamamoto, N., et al. (2014). The effect of lunar cycle, tidal condition and wind direction on the catches and profitability of Japanese common squid Todarodes pacificus jigging and trap-net fishing. *Fisheries Science, 80*(6), 1145–1157. https://doi.org/10.1007/s12562-014-0799-6.

Onea, F., & Rusu, E. (2012). Wind energy assessments along the Black Sea basin. *Meteorological Applications, 21*(2), 316–329. https://doi.org/10.1002/met.1337.

Özsoy, E., & Ünlüata, Ü. (1997). Oceanography of the Black Sea: a review of some recent results. *Earth-Science Reviews, 42,* 231–272.

Rusu, L., Bernardino, M., & Guedes Soares, C. (2014). Wind and wave modelling in the Black Sea. *Journal of Operational Oceanography, 7*(1), 5–20. https://doi.org/10.1080/1755876X.2014.11020149.

Rusu, L., Raileanu, A. B., & Onea, F. (2018). A comparative analysis of the wind and wave climate in the Black Sea along the shipping routes. *Water, 10*(7), 924–942. https://doi.org/10.3390/w10070924.

Saha, S., Moorthi, S., Pan, H., Wu, X., Wang, J., Nadiga, S., et al. (2010). The NCEP climate forecast system reanalysis. *Bulletin of the American Meteorological Society, 91,* 1015–1057. https://doi.org/10.1175/2010BAMS3001.1.

Saha, S., Moorthi, S., Wu, X., Wang, J., Nadiga, S., et al. (2014). The NCEP Climate Forecast System Version 2. *Journal of Climate, 27,* 2185–2208. https://doi.org/10.1175/JCLI-D-12-00823.1.

Salmi, T., Maatta, A., Anttila, P., Ruoho-Airola, T., & Amnell, T. (2002). Detecting trends of annual values of atmospheric pollutants by the Mann Kendall Test and Sen's slope estimates the excel template application MAKESENS. Finnish Meteorological Institute, Publications on Air Quality, No. 31, Helsinki.

Schlitzer, R. (2019). Ocean data view. https://odv.awi.de. Accessed 12 Oct 2019.

Sen, P. K. (1968). Estimates of the regression coefficient based on Kendall's Tau. *Journal of the American Statistical Association, 63,* 1379–1389.

Shadid, S. (2011). Trends in extreme rainfall events of Bangladesh. *Theoretical and Applied Climatology, 104*(3–4), 489–499. https://doi.org/10.1007/s00704-010-0363-y.

Shepherd, J. G., Brewer, P. G., Oschlies, A., & Watson, A. J. (2017). Ocean ventilation and deoxygenation in a warming

world: introduction and overview. *Philosophical Transactions of the Royal Society A: Mathematical, Physical and Engineering Sciences, 375,* 1–9. https://doi.org/10.1098/rsta.2017.0240.

Sterl, A., & Caires, S. (2005). Climatology, variability and extrema of ocean waves: the Web-based KNMI/ERA-40 wave atlas. *International Journal of Climatology*. https://doi.org/10.1002/joc.1175.

Stopa, J. S., & Cheung, K. F. (2014). Intercomparison of wind and wave data from the ECMWF reanalysis interim and the NCEP climate forecast system reanalysis. *Ocean Modelling, 75,* 65–83. https://doi.org/10.1016/j.ocemod.2013.12.006.

Surkova, G. V., Arkhipkin, V. S., & Kislov, A. V. (2013). Atmospheric circulation and storm events in the Black Sea and Caspian Sea. *Central European Journal of Geoscience, 5*(4), 548–559.

Troccoli, A., Muller, K., Coppin, P., Davy, R., Russell, C., & Hirsch, A. L. (2012). Long-term wind speed trends over Australia. *Journal of Climate, 25,* 170–183. https://doi.org/10.1175/2011JCLI4198.1.

Tuller, S. E. (2004). Measured WS trends on the west coast of Canada. *International Journal of Climatology, 24,* 1359–1374. https://doi.org/10.1002/joc.1073.

Valchev, N., Davidan, I., Belberov, Z., Palazov, A., & Valcheva, N. (2010). Hindcasting and assessment of the western Black sea wind and wave climate. *Environmental Protection and Ecology, 11*(3), 1001–1012.

Valchev, N., Trifonova, E., & Andreeva, N. (2012). Past and recent trends in the western Black Sea storminess. *Natural Hazards and Earth System Sciences, 12,* 961–977. https://doi.org/10.5194/nhess-12-961-2012.

Velea, L., Bojariu, R., & Cica, R. (2014). Occurrence of extreme winds over the Black Sea during January under present and near future climate. *Turkish Journal of Fisheries and Aquatic Sciences, 14,* 973–979. https://doi.org/10.4194/1303-2712-v14_4_17.

Wallace, J. M., & Gutzler, D. S. (1981). Teleconnections in the geopotential height field during the Northern hemisphere winter. *Monthly Weather Review, 109,* 784–812.

Wang, D. W., & Hwang, P. A. (2001). An operational method for separating wind sea and swell from ocean wave spectra. *Atmospheric Oceanic Technology, 18,* 2052–2062. https://doi.org/10.1175/1520-0426.

Weisse, R., & Gunther, H. (2007). Wave climate and long-term changes for the Southern North Sea obtained from a high-resolution hindcast 1958–2002. *Ocean Dynamics, 57,* 161–172. https://doi.org/10.1007/s10236-006-0094-x.

Young, I. R., Zieger, S., & Babain, A. (2011). Global trends in wind speed and wave height. *Science, 332*(6028), 451–455. https://doi.org/10.1126/science.1197219.

Zainescu, F., Tatui, F., Valchev, N., & Vespremeanu-Stroe, A. (2017). Storm climate on the Danube delta coast: evidence of recent storminess change and links with large-scale teleconnection patterns. *Natural Hazards, 87,* 599–621. https://doi.org/10.1007/s11069-017-2783-9.

Zecchetto, S., & de Biasio, F. (2007). Sea surface winds over the Mediterranean Basin from satellite data (2000–04): meso- and local-scale features on annual and seasonal time scales. *Journal of Applied Meteorology and Climatology, 46,* 814–827.

Zeng, X., Dickinson, R. E., & He, Y. (1998). Effect of surface sublayer on surface skin temperature and fluxes. *Journal of Climate, 11,* 537–550.

Zhang, D., Cronin, M. F., Wen, C., Xue, Y., Kumar, A., & McClurg, D. (2016). Assessing surface heat fluxes in atmospheric reanalyses with a decade of data from the NOAA Kuroshio Extension Observatory. *Journal of Geophysical Research: Oceans, 121,* 6874–6890. https://doi.org/10.1002/2016JC011905.

Zheng, C. W., Pan, J., & Li, C. Y. (2016). Global oceanic wind speed trends. *Ocean and Coastal Management, 129,* 15–24. https://doi.org/10.1016/j.ocecoaman.2016.05.001.

(Received March 19, 2019, revised October 14, 2019, accepted October 29, 2019, Published online November 11, 2019)